Journal of Molecular Structure 1295 (2024) 136746

Contents lists available at ScienceDirect

Journal of Molecular Structure

journal homepage: www.elsevier.com/locate/molstr

Neocuproine/nitrato complexes of Ni(II). Neutral and cationic species including salts with TCNQ: Preparation, chemical and spectroscopic properties and comparative structural chemistry

Slavomíra Šterbinská [a,c,*], Richard Smolko [a], Juraj Černák [a], Michal Dušek [b], Larry R. Falvello [c], Milagros Tomás [d]

[a] Department of Inorganic Chemistry, Faculty of Science, P. J. Šafárik University in Košice, Moyzesova 11, 041 54, Košice, Slovakia
[b] Institute of Physics of the Czech Academy of Sciences, Na Slovance 2, 182 21, Prague, Czech Republic
[c] Instituto de Nanociencia y Materiales de Aragón (INMA) and Departamento de Química Inorgánica, CSIC-Universidad de Zaragoza, Zaragoza, 50009, Spain
[d] Instituto de Síntesis Química y Catálisis Homogénea (ISQCH), Departamento de Química Inorgánica, Pedro Cerbuna 12, University of Zaragoza–CSIC, E-50009, Zaragoza, Spain

ARTICLE INFO

Keywords:
Nickel(II)
TCNQ
Neocuproine
NO_3^-
Crystal structure
Spectral properties

ABSTRACT

The cationic complex $[Ni(neoc)_2(NO_3)]^+$ with NO_3^- (**1**), $TCNQ^-$ (**3**), or $(TCNQ\text{-}TCNQ)^{2-}$ (**4**) as counterions, and the neutral complex $[Ni(neoc)([NO_3]^-\text{-}\kappa^1O)([NO_3]^-\text{-}\kappa^2O,O)(H_2O)]$ (**2**) can be obtained from different reactions involving Ni(II), *neoc*, NO_3^- and TCNQ. The molecular and extended crystal structure of compound **2**, which displays two different coordination modes for NO_3^-, are compared to those of the analogous Mn, Fe and Co compounds, revealing a correlation between the coordination geometry of the nominally monodentate nitrato ligand and the covalent radius of the central metal atom. Despite the differences in molecular geometry, the extended structures of the Ni (**2**) and Mn compounds are similar to each other but different from those of the Fe and Co complexes, which are similar to each other. Complex **1** was further used in the preparation of a new heterospin compound $[Ni(neoc)_2(NO_3)](TCNQ)$ (**3**), having an ionic structure with the same complex cation present in **1**, accompanied by centrosymmetric anion-radicals (ARs) $TCNQ^{\bullet-}$. Through a different preparation process, complex **4**, with the formula $[Ni(neoc)_2(NO_3)]_2(TCNQ\text{-}TCNQ)$, containing the same complex cation as in complexes **1** and **3**, but now with the centrosymmetric σ-dimerized dianion $(TCNQ\text{-}TCNQ)^{2-}$ has been obtained. The influence of NO_3^-, $TCNQ^{\bullet-}$ and $TCNQ\text{-}TCNQ^{2-}$ anions on the crystal structure of the cation $[Ni(neoc)_2(NO_3)]^+$ in the compounds has been studied. All of the complexes reported here have supramolecular structures governed by hydrogen bonding systems, adding to their stability.

1. Introduction

Organic anion radicals (ARs) occupy an interesting place in the landscape of heterospin systems from a physical and structural point of view. 7,7,8,8-Tetracyanoquinodimethanide anion-radical ($TCNQ^{\bullet-}$) formed by one-electron reduction of the neutral molecule TCNQ (Scheme 1) is one of the best-known ARs. An important characteristic of TCNQ is its ability to dimerize [1,2]. Although the π−dimerized form of $TCNQ^{\bullet-}$ is observed more often [3], the connection of two carbon atoms of ARs $TCNQ^{\bullet-}$ can lead to the formation of a σ−dimerized form, such as in the compound $[Ni(bpy)_3]_2(TCNQ–TCNQ)(TCNQ)_2{\cdot}6H_2O$ (*bpy* = 2, 2′-bipyridine) [4–5] or in $[Zn(bpy)(TCNQ–TCNQ)]_n$ [6]. The bond distance between the carbon atoms forming the dimerization σ−bond is in the range of 1.6 – 1.7 Å [1].

Beyond their structural properties, the physico-chemical properties of TCNQ complexes have been studied in depth. Their magnetic properties have been the subject of significant interest for decades [7,8]. An important milestone was the discovery of the first organic conductor TTF-TCNQ [9]. With the consequent interest in the conductivity of TCNQ compounds, these became frequent targets for attempts to form semiconducting charge-transfer systems [10]. To this end, several compounds of the type M-TCNQ, where M is a transition metal, were prepared, and two of them, semiconductors AgTCNQ and CuTCNQ, were studied in detail [11]. More recently, potentially important applications

* Corresponding author.
E-mail address: ssterbinska@unizar.es (S. Šterbinská).

https://doi.org/10.1016/j.molstruc.2023.136746
Received 26 June 2023; Received in revised form 19 September 2023; Accepted 27 September 2023
Available online 27 September 2023

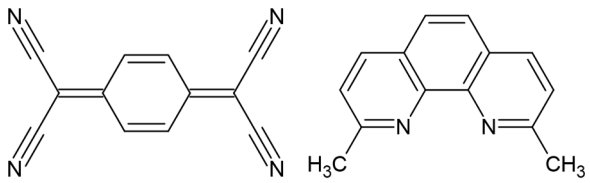

TCNQ molecule 2,9-dimethyl-1,10-phenanthroline (neocuproine)

Scheme 1. Chemical diagram of TCNQ and neocuproine.

of these compounds have emerged. TCNQ compounds have been reported for use in memory storage devices [12], as capacitors or porous materials [13], in gas sensing [14], as humidity sensors [15], in antibacterial materials [16], in catalysis [17] and in photocatalysis [18]. Because of the potential properties of TCNQ compounds, (gas adsorption, catalytic reactivity, charge transfer or conductivity), TCNQ became a useful redox-active linker in metal organic frameworks (MOF), such as in the case of Fe(TCNQ)(4,4′-*bpy*) [19]. Due to the π-stacking possibilities of TCNQ, it also participates in the formation of supramolecular structures [20] as in the case of $[Mn(TCNQ)_2(H_2O)_2]_\infty$ [21].

The study of compounds based on Ni(II) with TCNQ began in the middle of the last century. Despite the considerable interest in these magnetically and electrically attractive compounds [22–24], only 34 coordination compounds have been prepared and crystallographically characterized. Using the CSD [25] as a reference, it is evident that for preparation of heterospin complexes based on Ni(II) with TCNQ, N-donor [26–28] ligands were mainly used, and in a few cases, N,O- [29], N,S- [30], S- [31] and P-donor ligands were applied [32]. However, complexes with the "traditional" N-donor ligand *phen* (*phen* = 1, 10-phenanthroline) and its derivatives, e.g., *neoc* (*neoc* = neocuproine, 2,9-dimethyl-1,10-phenanthroline; Scheme 1) were not found.

All of the compounds described in this paper have one or two features in common, the major one being the presence of neocuproine as a ligand. The 2,9-dimethyl derivate of *phen, neoc* is more sterically demanding, which, among other things, makes it a useful ligand when preparing complexes in which we need to block some of the space on the central atom, resulting in the lowering of the coordination number. Several penta-coordinated Ni(II) complexes were prepared this way [33–35]. The ability of *neoc* to readily coordinate to the Ni(II) central atom is proven by the vast number of complexes of this nature found in the CSD. They range from tetra- to hexa-coordinate complexes, with either one or two molecules of *neoc* bonded to the central atom [36], with many mono-, di-, and up to tetranuclear complexes [37], which often combine more than one kind of central atom [38].

In the present work we also consider the *nitrato* ligand (NO_3^-) and its coordination modes in complexes. With three oxygen atoms, NO_3^- can act either as a monodentate ligand [39] or as a bridge connecting 2 or 3 central atoms [40]; and in the case of bidentate chelating of NO_3^- two donor oxygen atoms can be coordinated to one central metal [41]. More interesting are cases in which several coordination modes of the NO_3^- ligand co-exist in the same molecule, such as in the compound $[Co(NO_3)_2(neoc)(H_2O)]$ [42,43] where one NO_3^- ligand is monodentate, and the other chelates the central Co(II) atom.

In this work, we report the synthesis, characterization and crystal structures of two new precursors of heterospin compounds based on Ni (II) with neocuproine: $[Ni(neoc)_2(NO_3)](NO_3)\cdot CH_3CH_2OH\cdot 0.5H_2O$ (**1**) and $[Ni(neoc)([NO_3]^-\text{-}\kappa^1O)([NO_3]^-\text{-}\kappa^2O,O)(H_2O)]$ (**2**) along with the synthesis, characterization and crystal structure of new heterospin compounds formed by a combination of $TCNQ^{\bullet-}$ AR with the precursors mentioned above, namely $[Ni(neoc)_2(NO_3)](TCNQ)$ (**3**) and $[Ni(neoc)_2(NO_3)]_2(TCNQ\text{-}TCNQ)$ (**4**). To our knowledge, such heterospin systems have not previously been reported.

2. Experimental

2.1. Materials

$Ni(NO_3)_2\cdot 6H_2O$, neocuproine (98%), LiI (99.9%), TCNQ (98%), ethanol (99.8%), acetonitrile (99.9%), methanol (99.8%) and diethyl ether (99%) were purchased from commercial sources and used as received. LiTCNQ was prepared according to the published procedure [3].

2.2. Syntheses of complexes

2.2.1. $[Ni(neoc)_2(NO_3)](NO_3)\cdot CH_3CH_2OH\cdot 0.5H_2O$ (1) and $[Ni(neoc)([NO_3]^-\text{-}\kappa^1O)([NO_3]^-\text{-}\kappa^2O,O)(H_2O)]$ (2)

To an aqueous solution (5 ml) of nickel nitrate hexahydrate (0.1455 g, 0.5 mmol), 10 ml of an ethanolic solution of *neoc* (0.1041 g, 0.5 mmol) was added under constant stirring. The immediately formed pale blue precipitate was filtered off, dissolved in 10 ml of ethanol and left aside. Within a few days, dark blue plates of **1** crystallized, which were isolated from the bottom of the tube by filtration, washed with a small amount of ethanol and dried in air. The dried crystals of **1** evolved into a microcrystalline product **1a**. Blue block crystals of complex **2** were also isolated from this system, but mainly from the upper part of the same tube.

Anal. [%], calculated for $[Ni(neoc)_2(NO_3)](NO_3)\cdot CH_3CH_2OH\cdot 2.5H_2O$ (**1a**): C, 52.20; H, 4.54; N, 13.04; found: C, 52.22; H, 4.27; N, 12.77.

IR (cm^{-1}) of **1a**: 3416sh, 3060vw, 3019vw, 2924vw, 1621 m, 1593 m, 1567 m, 1511 w, 1497s, 1462vw, 1424 m, 1384s, 1358 w, 1297 m, 1284 m, 1220 w, 1202 w, 1156 m, 1101 w, 1029 m, 859 s, 840 w, 813 m, 808 m, 776 m, 747 w, 730 s, 681 m, 656 m, 551 s, 436 s.

IR (cm^{-1}) of **2**: 3412 m, 3254 m, 3066 w, 1674 m, 1622 m, 1595s, 1570 m, 1512 w, 1502 w, 1420 vs, 1377 w, 1362 m, 1310 vs, 1222 m, 1204 w, 1158 w, 1039 vs, 1001 m, 968 w, 861 vs, 845 m, 808 vs, 781 vs, 756 s, 730 vs, 693 w, 680 s, 660 m, 632 w, 549 vs, 459 s, 439 s, 412 s.

2.2.2. $[Ni(neoc)_2(NO_3)](TCNQ)$ (3)

To an aqueous solution of $Ni(NO_3)_2\cdot 6H_2O$ (0.3 mmol, 0.097 g, 3 ml), an ethanolic solution of *neoc* (0.6 mmol, 0.138 g, 5 ml) together with a methanolic solution of LiTCNQ (0.36 mmol, 0.084 g, 10 ml) were added. The reaction mixture in the flask was stirred for 10 min. The green microcrystalline product (0.21 g) of **3a** was isolated by filtration, washed with methanol and dried with ether.

IR (cm^{-1}) of **3a**: 3059 w, 3027 w, 2959 w, 2922 w, 2176 vs, 2148 vs, 2133 w, 1617 m, 1589 vs, 1565 m, 1495 w, 1477s, 1456 w, 1421 w, 1357 vs, 1321s, 1285 vs, 1219 m, 1202 w, 1182 vs, 1148s, 1028 vs, 853 vs, 838 vs, 809 vs, 775 s, 744 w, 729 vs, 697 w, 656 s, 615 w, 549 vs, 525 w, 494 vs, 460 w, 435 vs.

Anal. [%], found for **3a**: C, 64.81; H, 3.64; N, 16.99, calculated for this formula: $C_{40}H_{28}N_9NiO_3$: C, 64.80; H, 3.81; N, 17.00.

Single crystals of complex **3** suitable for X-ray study were prepared by a horizontal diffusion method [44]. 3 mg of solid LiTCNQ together with fresh insoluble crystals of complex **1** of approximate dimensions 0.4 × 0.4 × 0.2 mm were placed in a 30 mm diameter Petri dish with 2 ml of methanol. After 15 min, the resulting crystals of **3** were collected and analyzed.

IR (cm^{-1}) of **3**: 3061 w, 2174 vs, 2151 vs, 1619 m, 1592s, 1566 m, 1499s, 1477s, 1427s, 1375 m, 1357 vs, 1284 vs, 1221 m, 1206 m, 1181 m, 1155s, 1002 m, 855 vs, 830 vs, 813 m, 775 s, 744 w, 729 vs, 697 w, 681 s, 656 s, 615 w, 549 vs, 538 m, 483 vs, 460 w, 436 s.

2.2.3. $[Ni(neoc)_2(NO_3)]_2(TCNQ\text{-}TCNQ)$ (4)

Single crystals of **4** suitable for X-ray study were prepared by recrystallization of the microcrystalline powder sample of compound **3a** in acetone.

IR (cm^{-1}): 3052 w, 3025 w, 2958 w, 2925 w, 2171 vs, 2134 vs, 1706 m,1622 m, 1593 vs, 1567 m, 1496 m, 1474 m, 1427s, 1383 m, 1358 vs,

1322 vs, 1288 vs, 1221 vs, 1202 w, 1181 vs, 1163 m, 1152s, 1031 vs, 1012 m, 984 m, 941 m, 858 vs, 849 m, 808 vs, 776 vs, 746 m, 730 vs, 693 s, 680 s, 656 vs, 633 w, 616 w, 570 m, 549 vs, 525 vs, 500 vs, 462 w, 435 vs.

2.3. Physical measurements

CHN analysis of **1a** was performed on a vario MICRO instrument (Elementar Analysen systeme GmbH), and CHN analysis of **3a** was performed on a PerkinElmer 2400 Series II CHNS/O Analyser CHNS Elemental Analyzer. The IR spectrum of **1a** in the range 4000–400 cm^{-1} was recorded on a Nicolet 6700 FT-IR spectrophotometer from Thermo Scientific equipped with a diamond crystal Smart Orbit™, and the infrared spectra of **2** – **4** were recorded on FT-IR 4600 (Jasco) in the range 4000–400 cm^{-1}.

2.4. Single-crystal X-ray crystallography

Single-crystal X-ray data of complex **1** was collected on a SuperNova four-circle diffractometer equipped with AtlasS2 CCD detector and a microfocus mirror-collimated source utilizing CuKα radiation (λ = 1.54184 Å). Single-crystal X-ray data of complexes **2** – **4** were collected at low temperature (**2** also at room temperature, **2-RT**) on an Oxford Diffraction Xcalibur diffractometer equipped with a Sapphire 3 CCD detector and a graphite monochromator, utilizing MoKa radiation (λ = 0.71073 Å). The CrysAlis software package [45] was used for data collection and reduction. Absorption corrections were based on the multi-scan technique using ABSPACK [46]. The structures were solved by SHELXT [47] and refined against the F^2 data using full-matrix least-squares methods with the program SHELXL-2018/3 [48] incorporated in the WinGX program package [49]. Anisotropic displacement parameters were refined for all non-H atoms. Hydrogen atoms bonded to carbon atoms were placed in calculated positions and refined using a riding model with isotropic displacement parameters tied to those of their respective parent atoms (U_{iso}(H) = 1.2U_{eq}(C)). The structural figures were drawn using the program Diamond [50], and the chemical scheme was prepared using ACD/ChemSketch [51]. The program Mercury CSD 4.2.0 Development [52] was used to draw structure overlay figures. The crystal data and the final parameters of the structure refinements are summarized in Table 1; selected geometric parameters for **1** – **4** are given in Tables 2, 3, 6, and 7; and possible hydrogen bonds for **1** – **4** are given in Tables S1 – S5.

3. Results and discussion

3.1. Synthesis and identification

The reaction of $Ni(NO_3)_2{\cdot}6H_2O$ with neocuproine in a molar ratio 1:1 in a mixture of water with ethanol yielded a microcrystalline powder sample that, after recrystallization from ethanol produced dark blue plate crystals of $[Ni(neoc)_2(NO_3)](NO_3){\cdot}CH_3CH_2OH{\cdot}0.5H_2O$ (**1**). Blue polyhedral crystals of the complex $[Ni(neoc)([NO_3]^-\text{-}\kappa^1O)([NO_3]^-\text{-}\kappa^2O,O')(H_2O)]$ (**2**) were obtained as a minor component from the crystallization of compound **1**. It is worth noting that, unlike compound **2**, crystals of complex **1** are not stable in air, in which they evolved to a microcrystalline product **1a**, whose chemical analysis and IR agree with the formula $[Ni(neoc)_2(NO_3)](NO_3){\cdot}CH_3CH_2OH{\cdot}2.5H_2O$. Our effort to synthesize this hydrate (solvatomorph) directly was unsuccessful.

$[Ni(neoc)_2(NO_3)](TCNQ)$ (**3**) in the form of green crystals suitable for X-ray study was obtained by a fast horizontal diffusion reaction in methanol [44] of partially soluble LiTCNQ and insoluble crystals of$[Ni(neoc)_2(NO_3)](NO_3){\cdot}CH_3CH_2OH{\cdot}0.5H_2O$ (**1**). However, the reaction of nickel(II) nitrate dissolved in water, with neocuproine dissolved in ethanol and LiTCNQ dissolved in methanol in a molar ratio 1:2:1.2, that is, with all the reactants in solution, produced the dark-green microcrystalline product (**3a**). While the C, H, N analysis of the bulk solid (**3a**) agrees with the formula of **3**, the X-ray powder diffraction pattern did not identify of the microcrystalline powder sample **3a** with the

Table 2
Selected geometric parameters for **1** [Å, °]. Distances between the atoms generated through the symmetry operations are omitted.

Ni1-N1	2.056(3)	Ni2-N3	2.058(3)
Ni1-N2	2.112(3)	Ni2-N4	2.109(3)
Ni1-O1	2.148(3)	Ni2-O3	2.145(3)
O1-Ni1-O1^{i}	60.60(15)	O3-Ni2-O3^{ii}	60.21(17)
N1-Ni1-N2	80.68(13)	N3-Ni2-N4	81.02(13)

Symmetry codes: i: 1-x, y, 3/2-z; ii: -x, y, 3/2-z.

Table 1
Crystal data and structure refinement for **1 – 4**.

	1	2	2-RT	3	4
CSD number	2269677	2269673	2269675	2269674	2269672
Empirical formula	C30 H31 N6 O7.5 Ni	C14 H14 N4 O7 Ni	C14 H14 N4 O7 Ni	C40 H28 N9 O3 Ni	C80 H56 N18 O6 Ni2
Molecular weight	654.3	409.0	409.0	741.42	1482.84
Crystal system	Monoclinic	Monoclinic	Monoclinic	Triclinic	Monoclinic
Space group	*P*2/c	$P2_1/n$	$P2_1/n$	*P*-1	$P2_1/n$
Unit cell dimensions					
a (Å)	21.0008(8)	7.74389(14)	7.78909(16)	8.0446(2)	8.3470(3)
b (Å)	7.9118(2)	10.6496(2)	10.7771(2)	11.7545(4)	24.8936(8)
c (Å)	17.5529(6)	19.5811(3)	19.7718(4)	17.6161(4)	16.1928(6)
α (°)	90	90	90	89.601(2)	90
β (°)	94.444(3)	93.404(15)	93.5738(19)	89.442(2)	90.034(4)
γ (°)	90	90	90	86.288(3)	90
V (Å^3)	2907.72(17)	1611.99(5)	1656.49(6)	1662.18(8)	3364.6(2)
Z	2	4	4	2	2
D_{calc} (Mg.m^{-3})	1.495	1.685	1.640	1.481	1.464
Temperature (K)	95(2)	103(2)	295(2)	100(2)	100(2)
Crystal dimensions (mm)	0.105 × 0.095 × 0.046	0.226 × 0.082 × 0.068	0.206 × 0.067 × 0.047	0.240 × 0.087 × 0.031	0.215 × 0.049 × 0.016
θ range (°)	4.22 – 71.58	2.77 – 28.55	2.87 – 30.35	2.53 – 28.66	2.74 – 28.26
Reflections collected	9254	25,669	17,318	23,728	15,726
Independent reflections	9254	3771	4559	6882	7193
Goodness-of-fit on F^2	1.031	1.054	1.0001	1.032	1.005
R indices ($I > 2\sigma(I)$)	$R_1 = 0.0558$	$R_1 = 0.0302$	$R_1 = 0.0361$	$R_1 = 0.0499$	$R_1 = 0.0607$
	$wR_2 = 0.1468$	$wR_2 = 0.0665$	$wR_2 = 0.0790$	$wR_2 = 0.1058$	$wR_2 = 0.0945$
R indices (all data)	$R_1 = 0.0728$	$R_1 = 0.0394$	$R_1 = 0.0554$	$R_1 = 0.0749$	$R_1 = 0.1213$
	$wR_2 = 0.1557$	$wR_2 = 0.0716$	$wR_2 = 0.0883$	$wR_2 = 0.1202$	$wR_2 = 0.1147$
Diff. peak and hole (e·Å^{-3})	0.424; −0.493	0.335; −0.470	0.339; −0.350	0.532; −0.499	0.572; −0.684

Table 3
Selected geometric parameters for **2** at 103 K and for **2-RT** at 295 K [Å, °].

	2	2-RT
Ni1-N1	2.0483(14)	2.0516(15)
Ni1-N2	2.0617(15)	2.0567(16)
Ni1-O1	2.0488(13)	2.0568(15)
Ni1-O2	2.0519(12)	2.0588(14)
Ni1-O5	2.1740(12)	2.1746(14)
Ni1-O6	2.1124(12)	2.1201(14)
N1-Ni1-N2	82.32(6)	82.23(6)
O5-Ni1-O6	60.36(5)	59.78(6)

crystalline compound **3** (Fig. S1 in the Supplementary material). In order to prepare a pure bulk sample of **3**, the bulk microcrystalline **3a** was dissolved in acetone. The evaporation of the acetone solution produced crystals of a new compound, $[Ni(neoc)_2(NO_3)]_2$(TCNQ-TCNQ) (**4**). It was already noticed that $TCNQ^{\bullet-}$ AR [3] could evolve in solution, which is a limitation for the preparation/recrystallization of single crystals and/or pure bulk TCNQ compounds. The fast horizontal diffusion method [44] can produce single crystals by using a faster procedure than the typical recrystallization procedure and thus preventing the evolution of the $TCNQ^{\bullet-}$ AR. The preparation of **3** and **4** is a good example of the differences between these two techniques. Interestingly, the C, H and N analyses are identical for compounds **3, 4** and **3a**. Thus, compound **3a** could be a mixture of compounds **3** and **4**; however, the X-ray powder diffraction pattern of **3a** does not support this possibility. One possible explanation is that **3a** contains a polymorph of **3** or **4** with different X-ray powder diffractograms while having the same C, H and N analysis. Another possibility is the co-crystallization of $TCNQ^{\bullet-}$ AR and $TCNQ\text{-}TCNQ^{2-}$ with $[Ni(neoc)_2(NO_3)]$, as was observed in $[Ni(bpy)_3]_2(TCNQ–TCNQ)(TCNQ)_2{\cdot}6H_2O$ [4–5] and $[Ni(4,4'\text{-}dmbpy)_3]_2(TCNQ\text{-}TCNQ)(TCNQ)_2{\bullet}0.60H_2O$ [28]. There is also the possibility of coordinating the $TCNQ^{\bullet-}$ AR to the central Ni(II) atom. In this case, it should also change the coordination mode of the NO_3^- ligand (to monodentate instead of chelate) to keep the coordination index of the nickel center. As can be seen, different combinations can produce the observed analyses, showing the importance of the preparation of single crystals to determinate the nature of this solid.

The IR spectra of **1a–4** can be seen in Figs. 1-4. The tentative assignment of the observed absorption bands was done using literature data [53] and by comparison with the in-house measured IR spectrum of the ligand *neoc*. In the IR spectra of **1a** (Fig. 1) and **2** (Fig. 2)**,** broad shoulder bands are observed at around 3440 cm^{-1}, corresponding to the υ(O—H) vibrations from water molecules in the structures. This is followed by a group of low-intensity bands located at 3066, 3022 and 2967 cm^{-1} (**1a**) and 3035, 3008, 3002 and 2978 cm^{-1} (**2**), originating in *neoc* and representing $\upsilon(C_{ar}\text{-}H)$ and $\upsilon(C_{al}\text{-}H)$ types of vibrations. In the IR spectra of both compounds, three medium to strong sharp bands at around 1620, 1585 and 1536 cm^{-1} are present, typical for *neoc* and arising from $\upsilon(C_{ar}\text{-}N)$ and $\upsilon(C_{ar}\text{-}C_{ar})$ valence vibrations. From the lower region, we identified the band at 1386 cm^{-1} for **1a** and 1310 cm^{-1} for **2** as the deformation vibration $\delta_{as}(NO_3)$ of the nitrate groups. Symmetrical vibrations of this group ($\delta_s(NO_3)$) manifest themselves by a vibration band around 845 cm^{-1}. The last of the assigned bands is at 777 cm^{-1} for

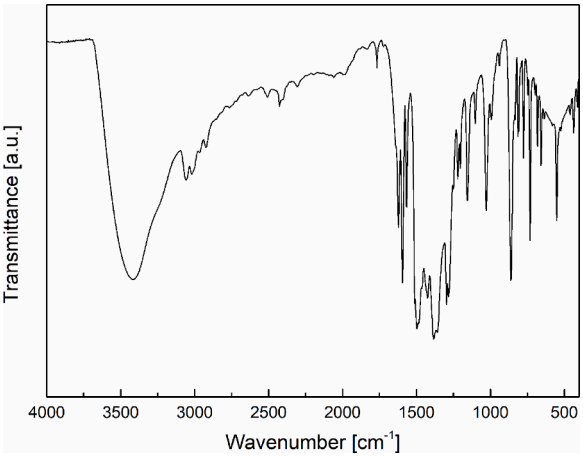

Fig. 1. IR spectrum of **1a**.

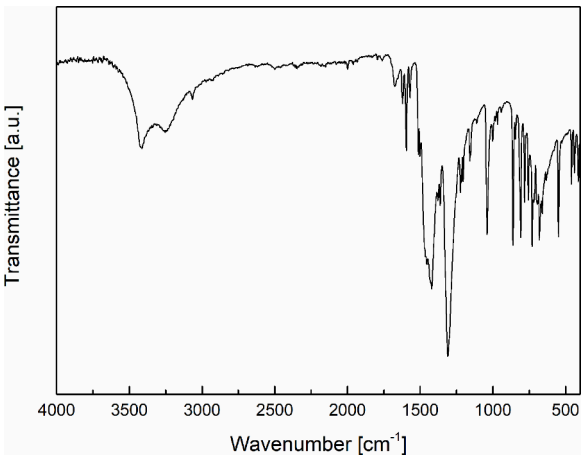

Fig. 2. IR spectrum of **2**.

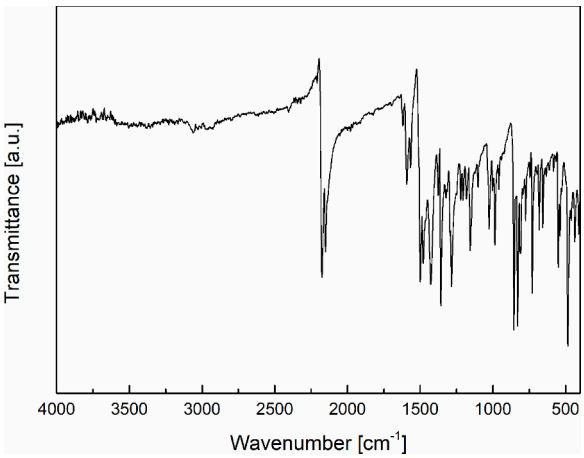

Fig. 3. IR spectrum of **3**.

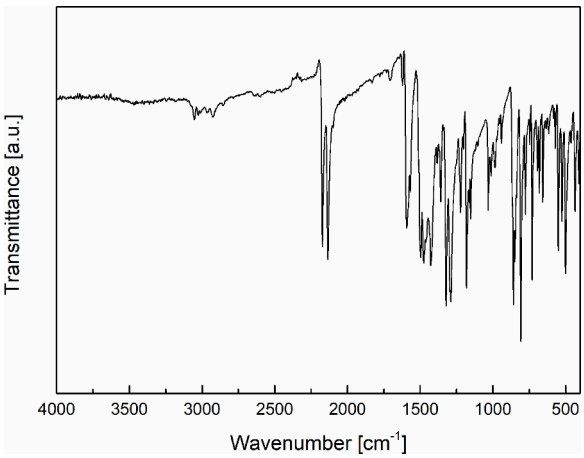

Fig. 4. IR spectrum of **4**.

1a and 781 cm^{-1} for **2**, identified as γ(C_{ar}-H).

In the IR spectra of crystals of compounds **3** (Fig. 3) and **4** (Fig. 4), the dominating absorption bands belong to valence vibrations υ(C≡N) from TCNQ groups. In both cases, two absorption bands are observed. For **3,** the positions of these bands were at 2174 and 2151 cm^{-1}; these values are typical of free, uncoordinated AR $TCNQ^{\bullet-}$ as in the compound [Ni(*dien*)$_2$](TCNQ)$_2$ (*dien* = 1,4,7-triazaheptane) [26]. In the IR spectrum of **4,** the two corresponding bands are located at 2171 and 2134 cm^{-1}. The position of the first absorption band is almost identical to that in the spectrum of **3**, but the second absorption band (2134 cm^{-1}) appears at lower wavenumbers as a consequence of the presence of a σ−dimerized $(TCNQ\text{-}TCNQ)^{2-}$ dianion. For comparison, the IR spectrum of compound **3a** was also measured (see **Figure S2** in SM). In the pertinent vibration region of C≡N groups, three absorption bands were observed at 2176, 2148 and 2133 cm^{-1}. These values again point out that compound **3a** can be a mixture of compounds **3** and **4** since similar values (2177, 2152 and 2138 cm^{-1}) were found in the IR spectrum of the compound [Ni(4,4′-*dmbpy*)$_3$]$_2$(TCNQ-TCNQ)(TCNQ)$_2$•0.60H_2O [28] which contains simultaneously free AR $TCNQ^{\bullet-}$ and σ−dimerized $(TCNQ\text{-}TCNQ)^{2-}$dianion, which also can be the case of **3a**. Strong absorption bands in the IR spectra of **3** and **4** originating from vibrations ν(C=C), ν(C−C), δ(C_{ar}−H), and ω($C(CN)_2$) were observed at around 1590 cm^{-1}, 1350 cm^{-1}, 825 cm^{-1} and 495 cm^{-1}. In the IR spectra of **3** and **4**, other absorption bands were also observed from *neoc* and *nitrato* ligands present in the complexes. For the *neoc* molecule, three weak absorption bands at around 3050, 3020 and 2950 cm^{-1} were identified as υ(C_{ar}-H) and υ(C_{al}-H) vibrations, along with the absorption bands at around 1620 cm^{-1} that belong to υ(C_{ar}-N). Absorption bands around 1320 cm^{-1} confirm the presence of the nitrate group in the compounds.

3.2. Crystal structures

The crystal structure of complex **1** (Fig. 5) is ionic, built up of [Ni(*neoc*)$_2$$(NO_3)$]$^+$ complex cations and nitrate anions for balancing the electroneutrality of the complex. In the outer coordination sphere, two solvate molecules exist simultaneously, ethanol and water. The chromophore is {NiN_4O_2}. Within the ethanol molecule, refinements indicated that one carbon atom was disordered, but further refinements of this disorder were unsuccessful. The oxygen atom O8 of the water molecule lies in a general position, and its occupancy was fixed at 0.5. It is worth noting that the crystal structure of **1** contains two crystallographically independent [Ni(*neoc*)$_2$$(NO_3)$]$^+$ cations, within both of which the Ni(II) central atoms are hexacoordinated with two chelate bonded *neoc* ligands and one *nitrato* ligand, which coordinates in bidentate chelating fashion. Moreover, the individual [Ni(*neoc*)$_2$$(NO_3)$]$^+$ complex cations are chiral, but the crystal structure, due to the presence of the center of symmetry (−1), is optically inactive. A search in the CSD did not yield any hits for [Ni(*neoc*)$_2$$(NO_3)$]$^+$. On the other hand, similar complex cations, namely [Ni(*phen*)$_2$$(NO_3)$]$^+$ and [Ni(*bpy*)$_2$$(NO_3)$]$^+$, have been reported, examples being [Ni(*phen*)$_2$$(NO_3)$]$(NO_3)$·4$H_2O$ [54] and [Ni(*bpy*)$_2$$(NO_3)$]$(NO_3)$ [55].

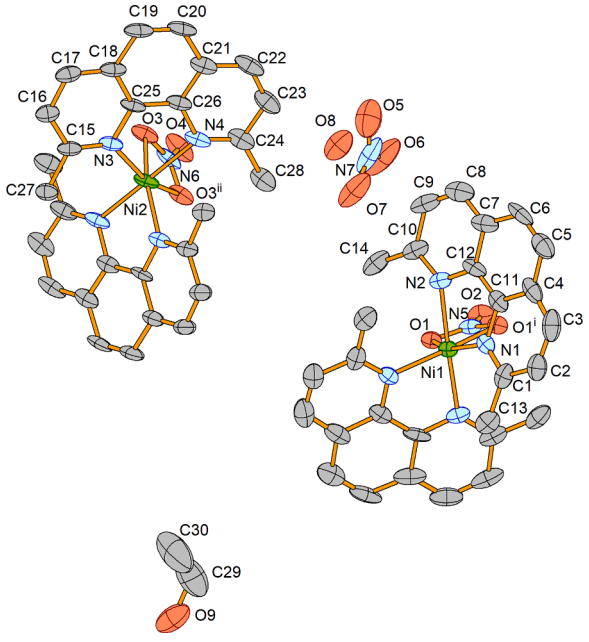

Fig. 5. View of the structure of complex **1**. Hydrogen atoms are omitted for clarity. The thermal ellipsoids are drawn at the 50% probability level. Symmetry codes: i: 1-x, y, 3/2-z; ii: -x, y, 3/2-z.

As concerns bond lengths, we observed marginal differences between the two complex cations; Ni-N bond lengths range from 2.056(3) Å to 2.112 (3) Å and Ni-O bond lengths are in the range of 2.145(3) Å to 2.148(3) Å (Table 2). Similar bond distances were observed in [Ni(*phen*)$_2$$(NO_3)$]$(NO_3)$·4$H_2O$ [54].

The supramolecular structure of **1** is governed by OH···X (*X* = O, N) hydrogen bonds linking the solvate molecules and nitrate anions (Fig. 6). The geometric parameters associated with hydrogen bonds are gathered in Table S1.

As can be seen from the packing of the structure of **1** in Fig. 7, ethanol solvate molecules are located between the planes of complex cations along the *c* axis in the structure, which enables their easy and relatively fast replacement with water molecules, as was the case in air dried crystals of **1** undergoing such a change to the microcrystalline powder of **1a**.

Compound **2** is neutral. Its crystal structure (Fig. 8) is formed by a Ni(II) central atom hexacoordinated by one N,N′-chelating *neoc* ligand, one O,O′-chelating *nitrato* ligand, one monodentate *nitrato* ligand and one aqua ligand *trans* to the monodentate nitrate. The chromophore is *cis*-{NiN_2O_4}. The observed Ni-N bond distances (Table 3) to the *neoc* ligand (2.0483(14) Å and 2.0617(15) Å) are within the expected range. As a consequence of the two different coordination modes of the *nitrato* ligands, it is possible to observe differences in Ni-O bond lengths. For the bidentate NO_3^- ligand, the Ni-O distances (2.1740(12) Å and 2.1124(12) Å) are longer than that for the monodentate NO_3^- ligand (2.0519(12) Å).

It is worth noting that two chemically isostructural compounds with the central atoms Co(II) and Fe(II) have been reported: [Co$(NO_3)_2$(*neoc*)(H_2O)] (KEQSAB, KEQSAB01) [42,43] and [Fe$(NO_3)_2$(*neoc*)(H_2O)] (QELZOX) [56]. Since their structures were determined at room temperature, for comparison, the crystal structure of **2** was also determined at room temperature (**2-RT**, see Table 1). Interestingly, despite their chemical isostructurality, the cell parameters of the Ni(II) compound **2-RT** are not similar to the cell parameters of the Co(II) compound KEQSAB (KEQSAB01) or the Fe(II) complex QELZOX (see Table 4), while the cell parameters of KEQSAB (KEQSAB01) and QELZOX are similar to each other. A related compound [Mn(*neoc*)$(NO_3)_2$$(H_2O)$] (TUSBIT) [57] was extracted from the CSD with similar cell parameters (Table 4) to those of complex **2-RT.** However, instead of the hexacoordinated central atom of Ni(II), the central atom is heptacoordinated in the Mn(II) compound, with chelating coordination for both *nitrato* ligands. Selected geometric parameters for these related compounds are shown in Table 5. It can be seen that the M-N bond distances to the *neoc* ligand increase along the series, as given in the table, from Ni(II) to Mn(II), in line with the increasing covalent radius of the metal. Thus, the larger covalent radius of Mn(II) allows heptacoordination, while in the smaller Ni(II), one of the two nitrates is monodentate. Co(II) and Fe(II) are intermediate, with some interaction between the metal atom and one of the non-coordinated oxygen atoms of the monodentate nitrate.

The supramolecular structure of **2** is established through O-H···O hydrogen bonds (**Table S2** for LT and **S3** for RT) connecting aqua ligands with monodentate as well as chelating *nitrato* ligands yielding a 2D arrangement (Fig. 9). It is interesting to note that one of the O-H···O

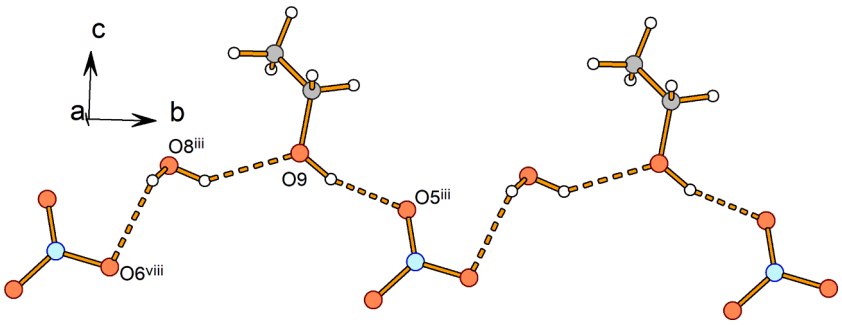

Fig. 6. Hydrogen bonding in **1**. For clarity, only atoms participating in hydrogen bonds are shown. Symmetry codes: iii: x, y, z-1; viii: x, y-1, z-1.

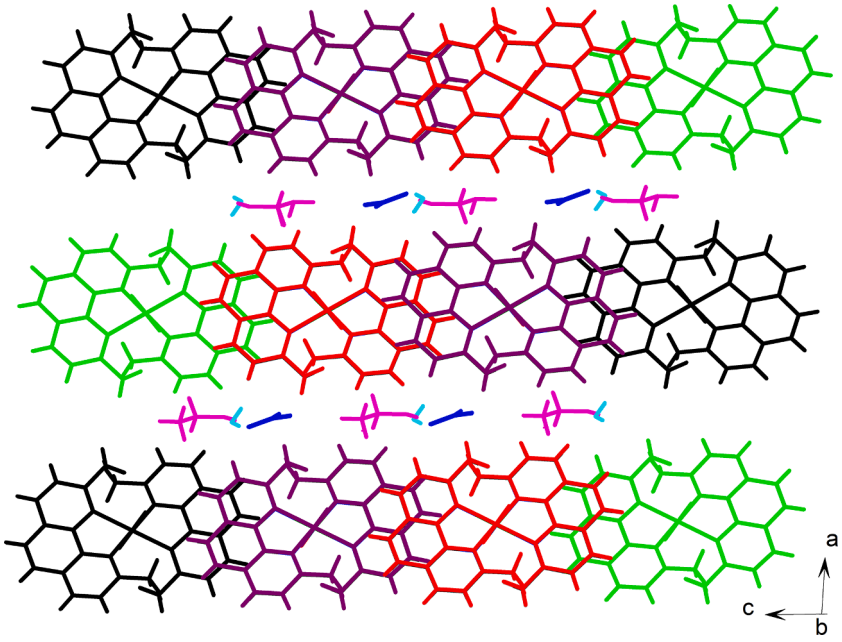

Fig. 7. View of the packing of the structure of **1**. Solvate molecules, along with the nitrate anions, are located between the planes of complex cations.

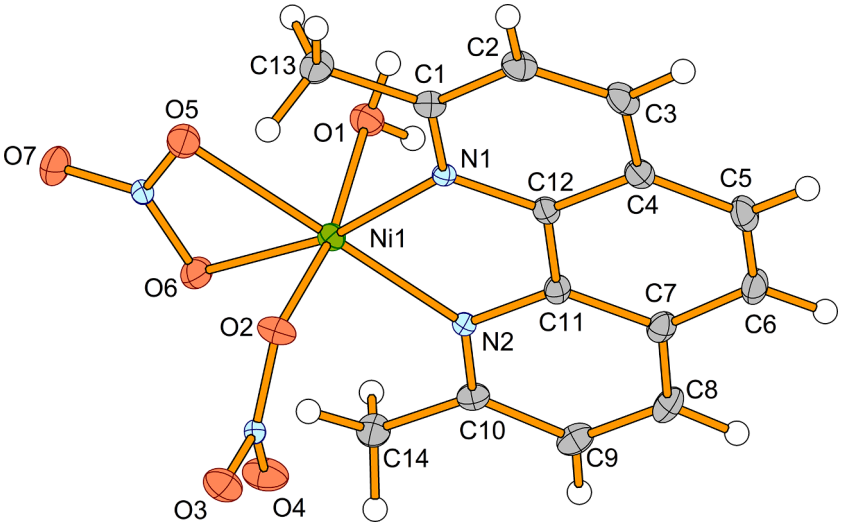

Fig. 8. Molecular structure of **2**. The thermal ellipsoids are drawn at the 50% probability level.

hydrogen bonds is bifurcated between two acceptor oxygen atoms, O3 and O4. In the analogous structures of the compounds $[Co(NO_3)_2(neoc)(H_2O)]$ [42,43] and $[Fe(NO_3)_2(neoc)(H_2O)]$ [56], although the same type of O-H···O hydrogen bonds can be observed, the supramolecular arrangement is different of that in **2** (Fig. 10). At the same time, the much weaker interactions of the C-H···O type are also present in both

Table 4
Selected crystal data for **2-RT**, KEQSAB, KEQSAB01, QELZOX and TUSBIT.

	Crystal system Space group	*a* (Å)	*b* (Å)	*c* (Å)	*β* (°)
2-RT (Ni)	Monoclinic $P2_1/n$	7.78909(16)	10.7771(2)	19.7718(4)	93.5738(19)
KEQSAB (Co)[#]	Monoclinic $P2_1/n$	11.1392	10.8081	14.7689	110.564
KEQSAB01 (Co)	Monoclinic $P2_1/n$	11.1529(15)	10.8072(9)	14.7733(19)	110.668(10)
QELZOX (Fe)[#]	Monoclinic $P2_1/n$	11.1447	10.8137	14.7734	110.548
TUSBIT (Mn)	Monoclinic $P2_1/n$	7.5244(5)	10.520(2)	20.806(3)	95.37(1)

[#] For comparison, the original space group $P2_1/c$ was transformed to $P2_1/n$.

Table 5
Selected geometric parameters for **2-RT**, KEQSAB, KEQSAB01, QELZOX and TUSBIT [Å, °].

	2-RT (Ni)	KEQSAB (Co)	KEQSAB01 (Co)	QELZOX (Fe)	TUSBIT (Mn)
r_{co} [58]	1.24(4)	1.26(3) ls	1.26(3) ls	1.32(3) ls	1.39(5) ls
r_{co} [58]	–	1.50(7) hs	1.50(7) hs	1.52(6) hs	1.61(8) hs
M-N1	2.0516(15)	2.112(2)	2.110(3)	2.115(2)	2.218(3)
M-N2	2.0567(16)	2.124(2)	2.124(3)	2.1244(19)	2.243(3)
M-O_w	2.0568(15)	2.067(2)	2.073(3)	2.077(2)	2.195(2)
M-O_{c1a}	2.1746(14)	2.309(2)	2.316(3)	2.310(2)	2.393(3)
M-O_{c1b}	2.1201(14)	2.130(2)	2.135(3)	2.133(2)	2.315(3)
M-O_{c2a}					2.242(2)
M-O_{c2b}					2.401(3)
M-O_t	2.0588(14)	2.211(3)	2.212(4)	2.213(2)	–
M···O_n	3.0559(2)	2.5657(5)	2.5693(4)	2.5706(3)	–

r_{co}: covalent radius, ls: low spin, hs: high spin, O_w: oxygen atom of the aqua ligand, O_t: oxygen atom of the monodentate *nitrato* ligand, O_c: oxygen atom of the chelating *nitrato* ligand, O_n: uncoordinated oxygen atom of the monodentate *nitrato* ligand.

mentioned structures. In the case of [Mn(*neoc*)$(NO_3)_2(H_2O)$] [57], only O-H···O hydrogen bonds are observed, while these bonds connect aqua ligands with both *nitrato* ligands in a similar way as in the structure of compound **2** (Fig. 11).

From Figs. 9–11, it is evident that three aqua ligands participate in the formation of similar supramolecular rings with descriptors $R_4^4(22)$ for **2** and $R_4^4(20)$ for [Mn(*neoc*)$(NO_3)_2(H_2O)$], while in the structures of [Co(*neoc*)$(NO_3)_2(H_2O)$] and [Fe(*neoc*)$(NO_3)_2(H_2O)$], two different supramolecular rings $R_2^2(12)$ and $R_6^6(32)$ are observed with two aqua ligands in the smaller one and four aqua ligands in the large one [59].

In the structure of **2**, it is possible to observe π-π interactions between the neighboring and coplanar aromatic rings from the *neoc* ligands (Fig. 12). The observed distance between Cg1 and $Cg1^{iv}$ (iv: 1-x, 1-y, 1-z) is 3.7153(1) Å at RT and 3.6671(1) at 103 K, where Cg1 is the centroid of the ring formed by the carbon atoms C4, C5, C6, C7, C11 and C12. Another longer distance (4.2792(1) Å at RT and 4.2663(1) at 103 K) was also found between centroids Cg1 and $Cg1^{v}$ (v: -x, 1-y, 1-z). However, this distance is too long to involve noncovalent π-π interactions [60]. Similar distances between the centroids were found in the previously mentioned compounds. For Co complex KEQSAB 3.564 Å [42], KEQSAB01 3.566(2) Å [43], Fe-containing QELZOX 3.572 Å [56] and Mn complex TUSBIT [57], the observed value is 3.577(2) Å.

It is interesting to notice that while the coordination sphere (bond lengths and coordination index) follows a clear relation with the covalent radii of the metal centers, the packing and the unit cell parameters do not show a similar relation; the Ni(II) and Mn(II) compounds present similar packing which is different to that of the Co(II) and Fe(II) compounds.

The crystal structure of **3** is ionic and is formed by the one crystallographically independent complex cation $[Ni(neoc)_2(NO_3)]^+$ and two halves of crystallographically independent $TCNQ^{\bullet-}$ ARs, giving a total ratio Ni/TCNQ of 1:1 (Fig. 13). In the complex cation, the Ni(II) center is coordinated by two neutral *neoc* ligands *via* four donor nitrogen atoms. The hexacoordination of Ni(II) is completed by one O,O′-chelating *nitrato* ligand. The Ni–N bond distances in compound **3** are in the range of 2.058 (2) to 2.107(2) Å (Table 6). The Ni–O distances are similar, with an average value of 2.1525(19) Å, and all these values correspond well with the bond distances observed in the precursor **1** used for preparing this complex. It is also important to note that no similar heterospin compound based on Ni(II) with $TCNQ^{\bullet-}$ ARs and the same *cis*-N_4O_2 donor set has been reported.

The observed C–N and C–C bond distances (Table 6) in the $TCNQ^{\bullet-}$ ARs correspond well to those observed for $[Ni(dien)_2](TCNQ)_2$ (*dien* = 1,4,7-triazaheptane) [26] which has two $TCNQ^{\bullet-}$ ARs per nickel atom in the structure. In complex **3**, two different types of bite angles can be observed. The larger angles are formed by the nitrogen donor atoms from the *neoc* ligand with the central atom of Ni(II) (average value is 80.94(8)°) and the smaller one (60.42(7)°) formed by the oxygen donor atoms from the *nitrato* ligand with the central atom of Ni(II) (Table 6). These are in the expected ranges for five- and four-membered chelates. For example, similar values of 80.4(3)° and 58.6(3)° were found in the structure of the dinuclear coordination compound [{Ru(*acac*)$_2$(CN)$_2$}{Ni(*neoc*)(NO_3)}]·H_2O (*acac* = acetylacetonate) [37].

The complex cations and $TCNQ^{\bullet-}$ ARs in **3** are connected via weak C-H···N interactions (**Table S4**), resulting in the formation of supramolecular chains (Fig. 14), which are not further connected.

In the chains, the alternation of two crystallographically independent $TCNQ^{\bullet-}$ ARs is observed. The first (type **A**) contains nitrogen atoms N6 and N7, and the second (type **B**) contains nitrogen atoms N8 and N9 (Fig. 14). The anion-radicals of the same type are parallel, but their distance (8.0446(2) Å) excludes the possibility of π-dimerization. For the same reason, the possibility of π-dimerization between the anion-radicals of types **A** and **B**, which form a dihedral angle of 25.19(78)°, is excluded. However, it is possible to observe π-π interactions between the aromatic rings from the *neoc* ligands of neighboring complex cations. These are parallel to each other, and the distance between the centroids Cg1 and $Cg1^{vi}$ (vi: -x, 1-y, 2-z) is 3.6045(1) Å, where Cg1 is the centroid of the ring formed by the carbon atoms C18, C19, C20, C21, C25 and C26 (Fig. 15).

Based on the bond lengths, it is possible to calculate the charge localized on the TCNQ units using the Kistenmacher relationship $\zeta = A\cdot[c/(b + d)] + B$, in which A and B are constants with the values of −41.667 and 19.833 respectively, and *b, c, d* are the respective bond lengths in the TCNQ unit (Scheme 2) [61]. Since compound **3** contains two crystallographically independent halves of $TCNQ^{\bullet-}$ ARs, two ζ values were calculated: ζ1 for $TCNQ^{\bullet-}$ AR type **A** and ζ2 for $TCNQ^{\bullet-}$ AR type **B** (Fig. 14). The calculated values $\zeta1 = -1.0078$ and $\zeta2 = -1.1141$ correspond to the expected values and support the conclusion that there is no electronic communication between the crystallographically independent $TCNQ^{\bullet-}$ ARs.

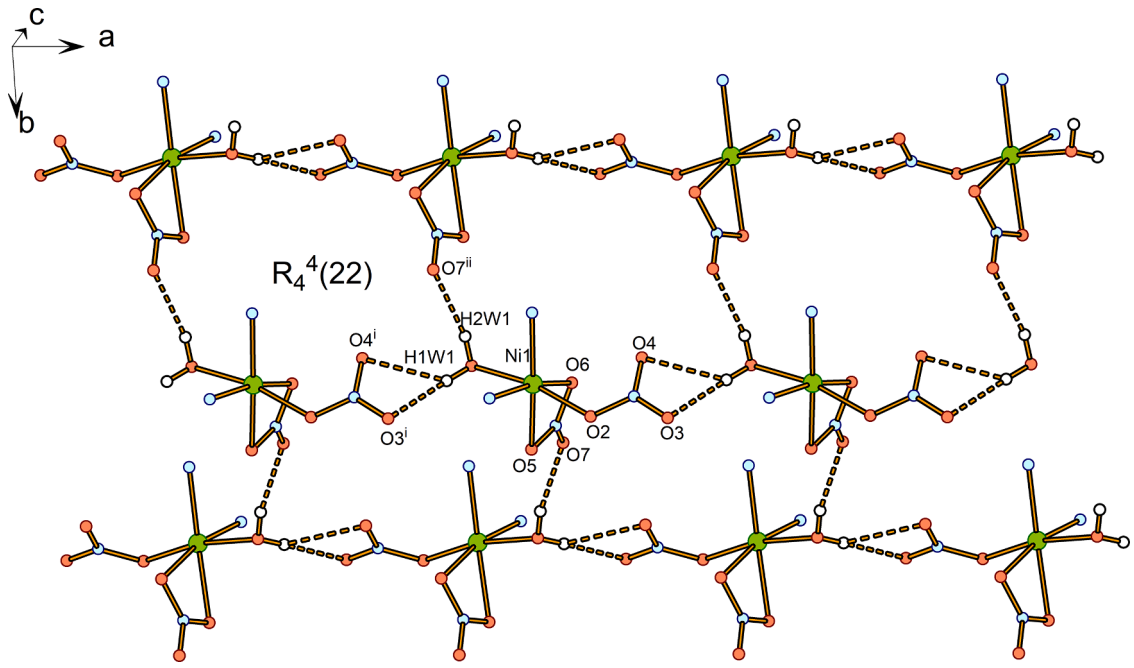

Fig. 9. Hydrogen bonding system in **2** (orange dashed lines). For clarity, only atoms participating in hydrogen bonds are shown. Symmetry codes: i: x-1, y, z; ii: 1/2-x, y-1/2, 3/2-z.

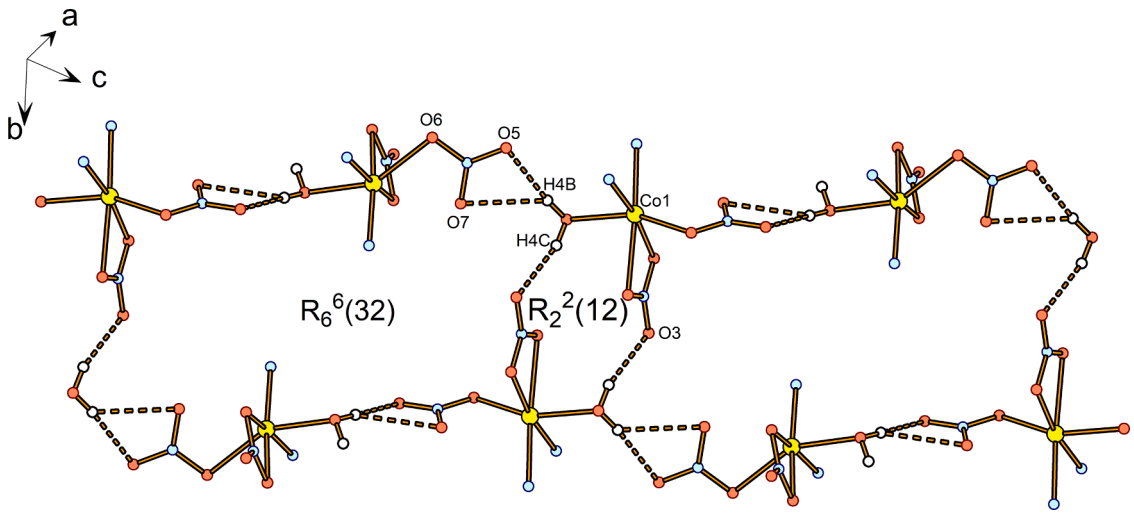

Fig. 10. Hydrogen bonding system in $[Co(NO_3)_2(neoc)(H_2O)]$ [42–43] (orange dashed lines). For clarity, only atoms participating in hydrogen bonds are shown.

The crystal structure of **4** is ionic, as in the case of complex **3,** and is formed by complex cations $[Ni(neoc)_2(NO_3)]^+$ and centrosymmetric σ-dimerized dianions $(TCNQ\text{-}TCNQ)^{2-}$ (Fig. 16). The complex cation is structurally identical to the previously described complex cation in compound **3**. The Ni–N bond distances are in the expected range, 2.051 (3) – 2.091(3) Å, and Ni–O distances are similar to the average value of 2.169 (2) Å; in this case, this bond is longer than for compound **3**. The chelate angles N1-Ni1-N2, N3-Ni1-N4 and O1-Ni1-O2 are almost identical to those observed in complex **3** (Table 7). The outstanding feature of this compound is the presence of the σ-dimerized dianion $(TCNQ\text{-}TCNQ)^{2-}$; we note that in complex **3**, TCNQ species were not dimerized, which means that acetone solution promotes dimerization. A similar phenomenon, solvent driven σ-dimerization of aryl dicyanomethyl radicals, was already observed [62]. The observed C–N and C–C bond distances (Table 7) in each TCNQ unit have expected values, but more significant is the value of the distance between carbon atoms C35 and $C35^i$ (1.643(6) Å). This value confirms the connection of TCNQ units and the formation of a σ-bond. A similar σ-dimerized dianion $(TCNQ\text{-}TCNQ)^{2-}$ was observed in the structure of the compound $[Cu(DMP)_2]_2[TCNQ]_2$ (DMP = *neoc*) [63]. It is worth noting that until now, only two coordination compounds, $[Ni(bpy)_3]_2(TCNQ–TCNQ)(TCNQ)_2{\cdot}6H_2O$ [4–5] and $[Ni(4,4'\text{-}dmbpy)_3]_2(TCNQ\text{-}TCNQ)(TCNQ)_2{\bullet}0.60H_2O$ [28], based on Ni(II) with π- and also σ-dimerized TCNQ units have been prepared.

It is also interesting to compare the angles around the carbons C31 and C37 in complex **3** with those around carbon C35 in complex **4**. Table 8 shows the influence of the hybridization of the carbon atoms on the values of the angles in each compound. In compound **3,** the carbons C31 and C37 are sp^2 hybridized with the angles within the expected range, while in complex **4,** the sp^3 hybridization of carbon atom C35 corresponds to the expected smaller angles.

The 2D supramolecular structure of **4** is formed by weak C-H···N interactions (**Table S5**), thanks to which each σ-dimerized dianion $(TCNQ\text{-}TCNQ)^{2-}$ is connected with four different complex cations [Ni

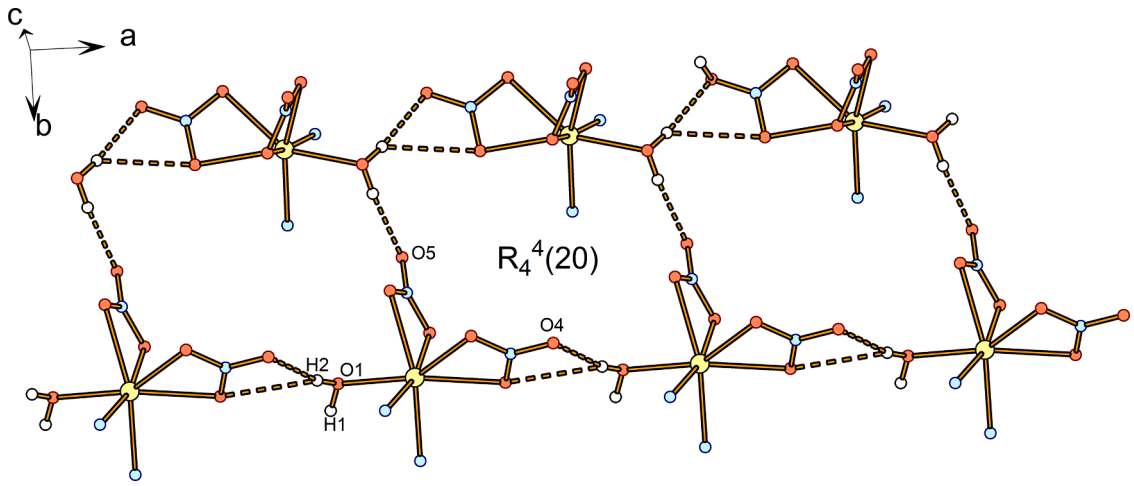

Fig. 11. Hydrogen bonding system in [Mn(*neoc*)$(NO_3)_2(H_2O)$] [57] (orange dashed lines). For clarity, only atoms participating in hydrogen bonds are shown.

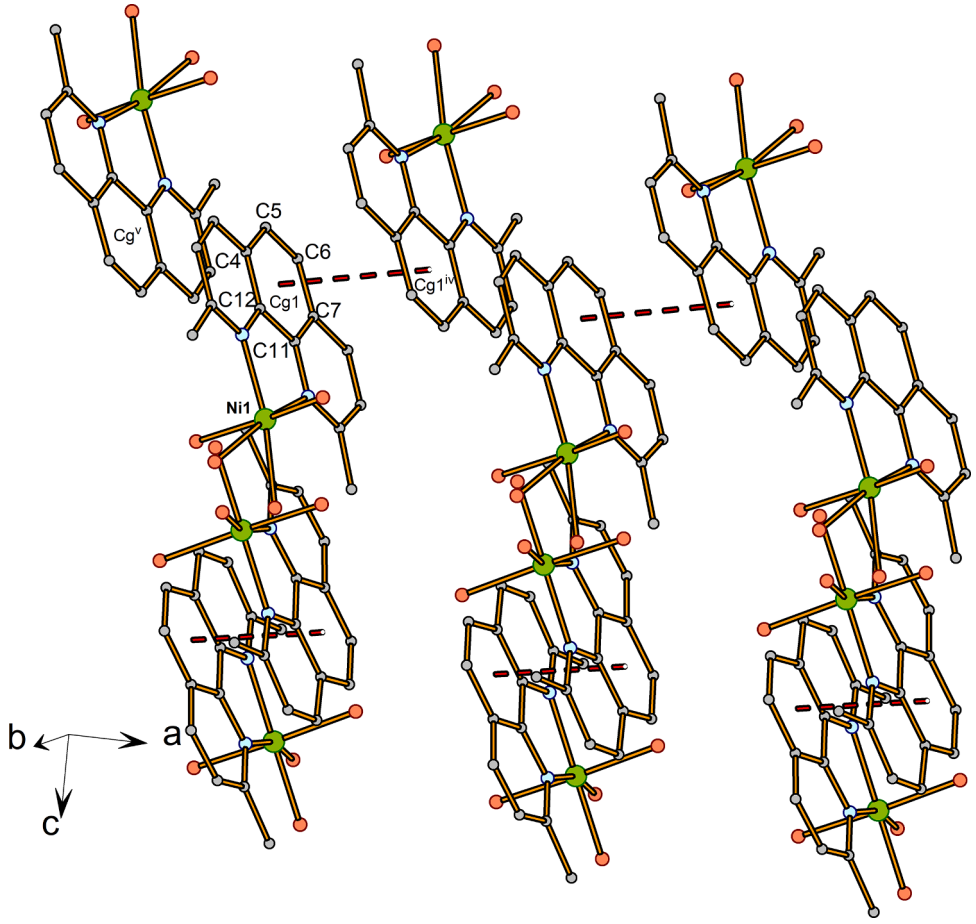

Fig. 12. View of π-π interactions between aromatic rings from the *neoc* ligands (red dotted line) in the structure of complex **2**. Hydrogen atoms are omitted for clarity. Symmetry codes: iv: 1-x, 1-y, 1-z, v: -x, 1-y, 1-z.

(*neoc*)$_2(NO_3)]^+$ through its nitrogen atoms. In the structure, only one extensive supramolecular ring is observed, which can be described by the descriptor R_4^4 (42) (Fig. 17).

The compounds **1, 3** and **4** contain the same complex cation [Ni(*neoc*)$_2(NO_3)]^+$, allowing us, using the Mercury program [52], to compare the shapes and geometric parameters of the individual complex cations and assess differences caused by crystal packing forces (presence of counter anion, intermolecular interactions with the solvate molecules). Six comparisons were made, namely **1A** (blue) – **1B** (violet), **1A** – **3** (red), **1A** – **4** (green), **1B** – **3, 1B** – **4** and **3** – **4** (Fig. 18 and **Figure S3**), where **1A** and **1B** are as the complex cations of **1** containing the central atom Ni1 and Ni2, respectively. It can be seen that the pairs **1A** - **1B** and **1A** - **3** are almost identical, **1A** – **4** and **1B** – **3** differ only slightly, and some differences can be observed in **1B** – **4** and **3** – **4**. The RMSD (root mean square deviation) values range between 0.0478 and 0.2062, and the values for the Max. D (maximum distance between

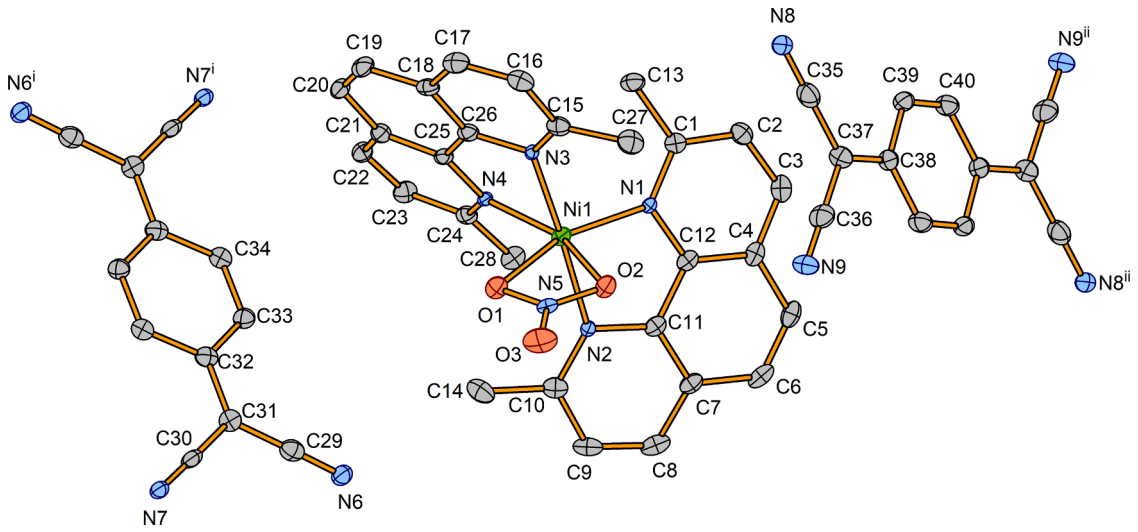

Fig. 13. View of the structure of complex **3**. Hydrogen atoms are omitted for clarity. The thermal ellipsoids are drawn at the 50% probability level. Symmetry codes: i: 1-x, -y, 2-z; ii: -x, 2-y, 1-z.

Table 6
Selected geometric parameters for **3** [Å, °].

Ni1-N1	2.062(2)	C33-C34	1.361(4)
Ni1-N2	2.105(2)	C36-C37	1.415(4)
Ni1-N3	2.107(2)	C35-C37	1.424(4)
Ni1-N4	2.058(2)	C35-N8	1.152(3)
Ni1-O1	2.1457(18)	C36-N9	1.154(4)
Ni1-O2	2.1592(19)	C37-C38	1.428(4)
C29-C31	1.420(4)	C38-C39	1.421(4)
C30-C31	1.420(4)	C39-C40	1.361(4)
C29-N6	1.153(3)	N1-Ni1-N2	80.87(8)
C30-N7	1.147(3)	N3-Ni1-N4	81.00(8)
C31-C32	1.419(4)	O1-Ni1-O2	60.42(7)
C32-C33	1.417(4)		

equivalent atoms) are in the range of 0.0827 – 0.4429 Å.

In the same way, the overlay of **2** with the structure of [Mn(*neoc*)$(NO_3)_2(H_2O)$] was done (Fig. 19) to assess the influence of different coordination modes of two *nitrato* ligands (monodentate and chelate bonded in **2**, both chelate-bonded in [Mn(*neoc*)$(NO_3)_2(H_2O)$]). Fig. 19 shows, as expected, a good correspondence between the chelate-bonded NO_3^- ligands, and a significant difference between the chelate and monodentate-bonded ligands.

4. Conclusions

Two new coordination compounds from the water-ethanolic solution of $Ni(NO_3)_2{\cdot}6H_2O$ and neocuproine were prepared, namely [Ni(*neoc*)$_2(NO_3)$]$(NO_3){\cdot}CH_3CH_2OH{\cdot}0.5H_2O$ (**1**) and [Ni(*neoc*)($[NO_3]^-$-κ^1O)($[NO_3]^-$-κ^2O,O')(H_2O)] (**2**); also, two new coordination compounds with nitrate, neocuproine and TCNQ were obtained: [Ni(*neoc*)$_2(NO_3)$](TCNQ) (**3**) with $TCNQ^{\bullet-}$ AR and [Ni(*neoc*)$_2(NO_3)]_2$(TCNQ-TCNQ) (**4**) with σ-dimerized $(TCNQ)_2^{2-}$. Compound **3** results from two reaction steps consisting of the preparation of the crystals of complex **1** followed by its reaction with LiTCNQ, while compound **4** is obtained when the reaction is done in just one step: reaction of $Ni(NO_3)_2{\cdot}6H_2O$ with neocuproine and LiTCNQ, and recrystallization in acetone. These results agree with our previously reported method [44] for obtaining crystals of compounds with the $TCNQ^{\bullet-}$ AR. When the formation of the crystal is fast using an insoluble crystalline starting material, compound **1** in this case, it is possible to obtain a new compound with $TCNQ^{\bullet-}$ AR (**3**). In contrast, the recrystallization of the TNCQ-containing compound, **3a**, as is known, can produce the degradation/evolution of the $TCNQ^{\bullet-}$ AR. In the present study, we identified the nature of this evolution. The synthesis and structural characterization of compound **4** indicate that the evolution of the $TCNQ^{\bullet-}$ AR can lead to the σ-dimerized $(TCNQ)_2^{2-}$, which is no longer radical. Compounds **3** and **4** are good examples for comparing the two different crystallization techniques.

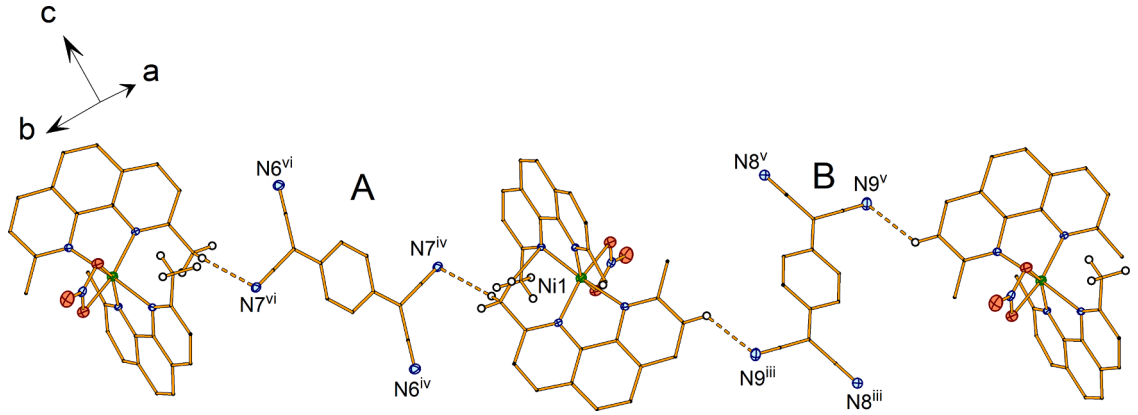

Fig. 14. View of the weak C—H···N interactions (orange dashed lines) in the structure of complex **3**. For clarity, hydrogen atoms that do not participate in the system of weak interactions are omitted. The thermal ellipsoids are drawn at the 50% probability level. Symmetry codes: iii: 1-x, 1-y, 1-z; iv: x-1, y + 1, z; v: x + 1, y-1, z; vi: -x, 1-y, 2-z.

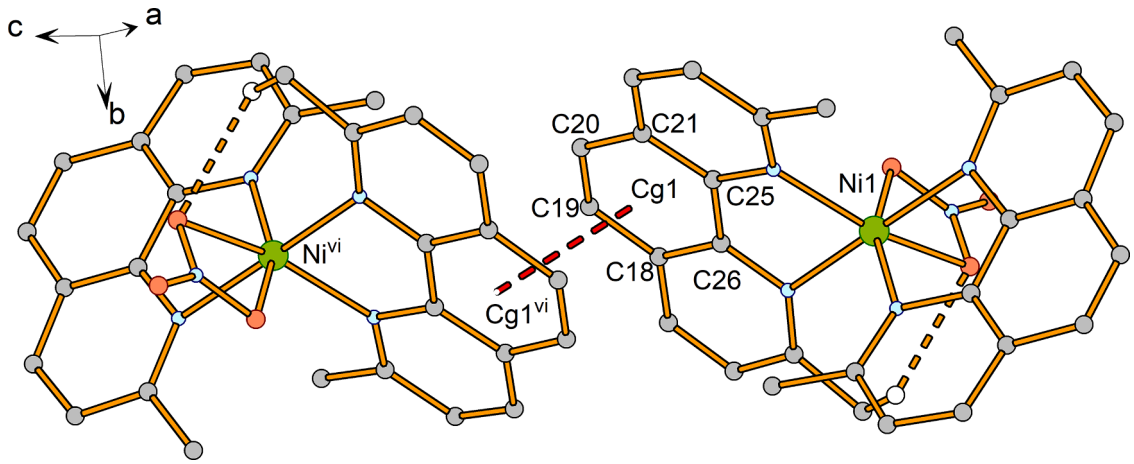

Fig. 15. View of π-π interaction between aromatic rings from the *neoc* ligands (red dotted line) in the structure of complex **3**. Hydrogen atoms, except those involved in interactions, are omitted for clarity. Symmetry code: vi: -x, 1-y, 2-z.

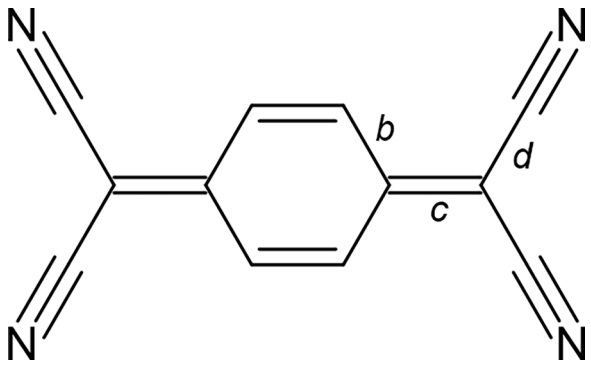

Scheme 2. TCNQ molecule with assignated bonds.

From the structures of these four newly prepared coordination compounds with *nitrato* and *neoc* ligands, some further conclusions can be obtained by comparing them with previously reported compounds.

Three complexes, **1, 3** and **4,** are ionic, built up of the same complex cation $[Ni(neoc)_2(NO_3)]^+$ and three different counterions NO_3^- (**1**), $TCNQ^{\bullet -}$ (**3**) and TCNQ-$TCNQ^{2-}$ (**4**). In the complex cation, the central atom of Ni(II) is hexacoordinated by two *neoc* ligands and one *nitrato* ligand. These anions almost do not modify the shape and bond distances of $[Ni(neoc)_2(NO_3)]^+$; however, they influence the crystal stability.

Table 7
Selected geometric parameters for **4** [Å, °].

Ni1-N1	2.051(3)	C35-C37	1.482(4)	C38-C40	1.417(5)
Ni1-N2	2.091(3)	C37-N7	1.143(4)	C40-N9	1.153(4)
Ni1-N3	2.069(3)	C29-C30	1.400(5)	C38-C39	1.413(5)
Ni1-N4	2.069(3)	C30-C31	1.371(4)	C39-N8	1.154(4)
Ni1-O1	2.207(2)	C31-C32	1.409(4)	C35-C35^i	1.643(6)
Ni1-O2	2.131(2)	C32-C33	1.410(5)	N1-Ni1-N2	81.06(11)
C29-C35	1.521(4)	C33-C34	1.377(4)	N3-Ni1-N4	81.40(10)
C35-C36	1.472(5)	C29-C34	1.400(4)	O1-Ni1-O2	59.60(8)
C36-N6	1.143(4)	C32-C38	1.441(4)		

Symmetry code: i: 1-x, 1-y, 1-z.

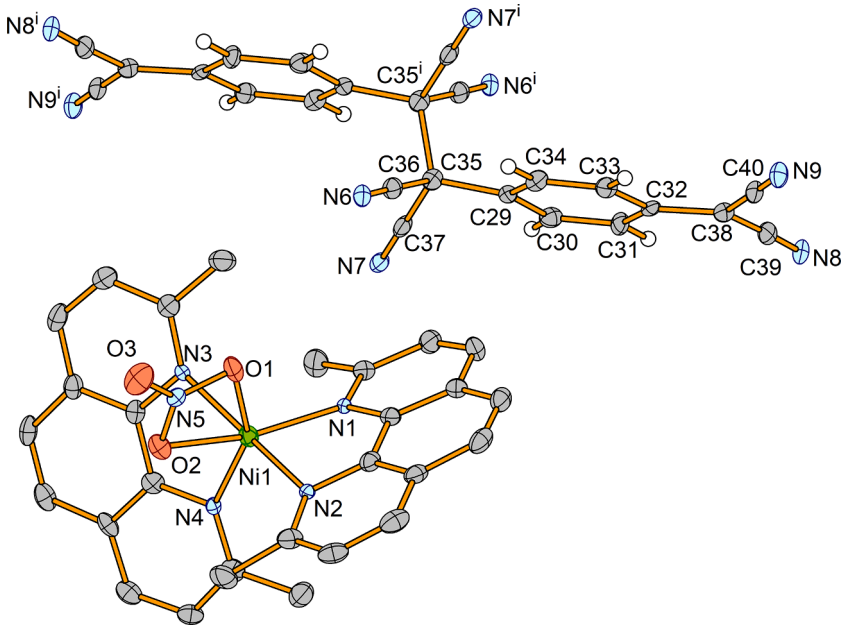

Fig. 16. View of the structure of complex **4**. For clarity, only one crystallographically independent complex cation is shown, and the hydrogen atoms of the complex cation are omitted. The thermal ellipsoids are drawn at the 50% probability level. Symmetry code: i: 1-x, 1-y, 1-z.

Table 8
Selected angles for **3** and **4** [°].

3 (sp^2 hybridization)		**4** (sp^3 hybridization)	
C30-C31-C32	121.2(2)	C29-C35-C37	111.9(3)
C36-C37-C38	121.6(2)		
C29-C31-C32	122.3(2)	C29-C35-C36	110.9(3)
C35-C37-C38	121.4(2)		
C35-C37-C36	116.9(2)	C36-C35-C37	107.1(3)
		C29-C31-C30	116.4(2)
		$C35^{i}$-C35-C36	107.5(3)
		$C35^{i}$-C35-C37	106.7(3)
		$C35^{i}$-C35-C29	112.4(3)

Symmetry code: i: 1-x, 1-y, 1-z.

While **3** and **4** are stable, compound **1** is unstable due to the presence of rather volatile ethanol solvate molecules in the open space between the planes of complex cations in the crystal structure. Complex **2** is neutral and is formed by the central atom of Ni(II) coordinated by one *neoc* ligand, two *nitrato* ligands and one aqua ligand. The comparison of [Ni(*neoc*)($[NO_3]^-$-κ^1O)($[NO_3]^-$-κ^2O,O')(H_2O)] (**2**) with related [M(*neoc*)(NO_3)$_2$(H_2O)] (M=Co, Fe, Mn) compounds shows that the M-(*nitrato*-κ^1O) evolves from monodentate (*M*=Ni) to bidentate M-(*nitrato*-κ^2O,O') (*M*=Mn), in accord to the increase in the covalent radii, and therefore going from a coordination number of 6 (*M*=Ni) to 7 (*M*=Mn). The Co(II) and Fe(II) compounds have an intermediate behavior. However, the Ni and Mn compounds, which have the most different molecular structures (coordination index 6 and 7, respectively), present the same molecular packing, while Co(II) and Fe(II) pack in different ways. The supramolecular structures of **1** and **2** are established by hydrogen-bonding systems based on O—H···O hydrogen bonds, and in the case of complex **2**, also π−π interactions between aromatic rings from *neoc* ligands are observed. In contrast, the supramolecular structure of **3** and **4** is formed by a hydrogen bonding system based on C–H···N hydrogen bonds.

CRediT authorship contribution statement

Slavomíra Šterbinská: Investigation, Visualization, Validation, Writing – original draft, Writing – review & editing. **Richard Smolko:** Investigation, Visualization, Writing – original draft. **Juraj Černák:** Supervision, Conceptualization, Writing – review & editing, Project administration, Funding acquisition. **Michal Dušek:** Investigation, Data curation, Formal analysis, Writing – review & editing, Project administration, Funding acquisition. **Larry R. Falvello:** Investigation, Data curation, Formal analysis, Writing – review & editing, Project administration, Funding acquisition. **Milagros Tomás:** Supervision, Conceptualization, Validation, Writing – review & editing.

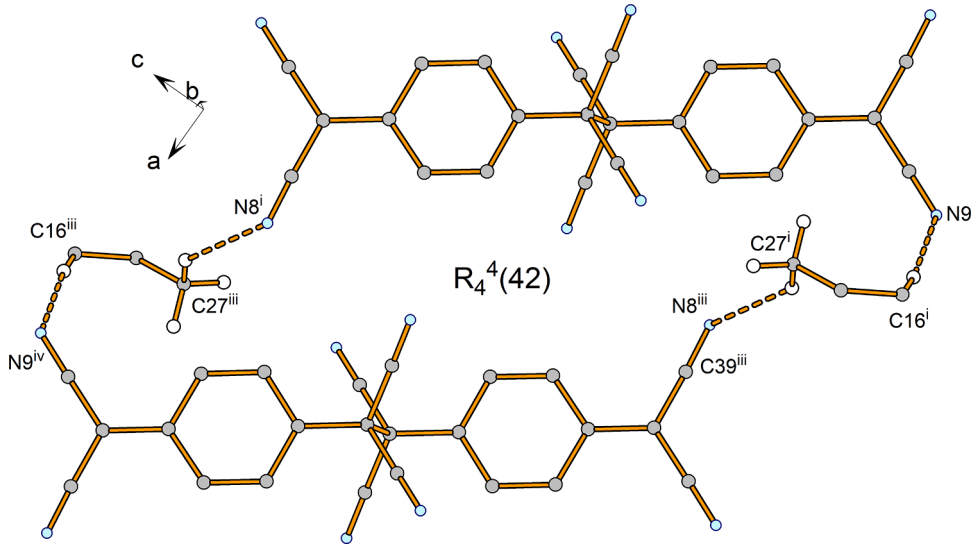

Fig. 17. View of the interactions (orange dashed lines) in the structure of compound **4**. For clarity, hydrogen atoms not involved in weak interactions are omitted. Symmetry codes: i: 1-x, 1-y, 1-z; iii: x + 1, y, z; iv: 2-x, 1-y, 1-z.

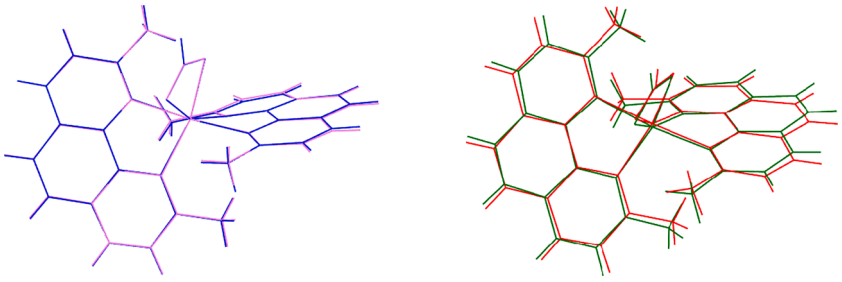

1a and **1b**

RMSD = 0.0478

Max. D = 0.0827

3 and **4**

RMSD = 0.1978

Max D = 0.3558

Fig. 18. The overlays **1A** – **1B** and **3** – **4** of the complex cations [Ni(*neoc*)$_2$(NO_3)]$^+$. RMSD is Root Mean Square Deviation, and Max. D is the maximum distance between two equivalent atoms.

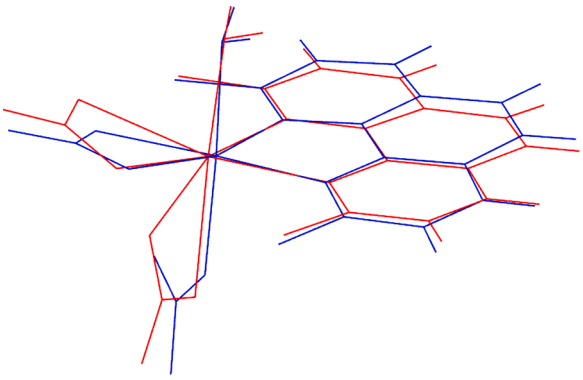

Fig. 19. The overlay of the structure **2** (blue) and [Mn(*neoc*)$(NO_3)_2(H_2O)$] (red) with RMS 0.102, where RMS is Root Mean Square. Hydrogen atoms from methyl groups are omitted for clarity.

Declaration of Competing Interest

The authors declare that they have no known competing financial interests or personal relationships that could have appeared to influence the work reported in this paper.

Data availability

The crystallographic data can be obtained free of charge via http://www.ccdc.cam.ac.uk/conts/retrieving.html.

Acknowledgements

This work was supported by the Slovak Grants (APVV-18–0016, VEGA 1/0189/22), Internal Grant of the Faculty of Science of Pavol Jozef Šafárik University (VVGS-PF-2022–2140) and by the Spanish Ministerio de Ciencia e Innovación (Grant PID2021–124880NB-I00), the European Union Regional Development Fund, (FEDER), and the Diputación General de Aragón, Project M4, E11_20R. Crystallography partly (compound **1**) used the Czech Nanolab infrastructure supported by MEYS CR (LM2023051).

Supplementary materials

Supplementary material associated with this article can be found, in the online version, at doi:10.1016/j.molstruc.2023.136746.

References

[1] J. Huang, S. Kingsbury, M. Kertesz, Crystal packing of TCNQ anion π-radicals governed by intermolecular covalent π–π bonding: DFT calculations and statistical analysis of crystal structures, Phys. Chem. Chem. Phys. 10 (2008) 2625–2635, https://doi.org/10.1039/b717752f.

[2] A.L. Sutton, B.F. Abrahams, D.M. D'Alessandro, T.A. Hudson, R. Robson, P.M. Usov, Structural and optical investigations of charge transfer complexes involving the radical anions of TCNQ and F_4TCNQ, CrystEngComm 18 (2016) 8906–8914, https://doi.org/10.1039/c6ce02015a.

[3] L.R. Melby, R.J. Harder, W.R. Hetler, W. Mahler, R.E. Benson, W.E. Mochel, Substituted quinodimethans. II. Anion-radical derivatives and complexes of 7,7,8,8-tetracyanoquinodimethan, J. Am. Chem. Soc. 84 (1962) 3374–3387, https://doi.org/10.1021/ja00876a029.

[4] J. Černák, J. Kuchár, M. Hegedüs, Disorder of the dimeric TCNQ-TCNQ unit in the crystal structure of $[Ni(bpy)_3]_2$(TCNQ-TCNQ)-$(TCNQ)_2{\cdot}6H_2O$ (TCNQ is 7,7,8,8-tetracyanoquinodimethane), Acta Cryst E73 (2017) 8–12, https://doi.org/10.1107/S2056989016019162.

[5] S. Šterbinská, M. Holub, M. Hegedüs, J. Titiš, E. Čižmár, L.R. Falvello, J. Černák, Temperature-dependent dimerization of TCNQ anion-radical in $[Ni(bpy)_3]_2$(TCNQ–TCNQ)$(TCNQ)_2{\cdot}6H_2O$: single-crystal structure, magnetic and quantum chemical study, Solid State Sci. 131 (2022), 106959, https://doi.org/10.1016/j.solidstatesciences.2022.106959.

[6] S. Shimomura, R. Matsuda, S. Kitagawa, Flexibility of porous coordination polymers strongly linked to selective sorption mechanism, Chem. Mat. 22 (2010) 4129–4131, https://doi.org/10.1021/cm101410h.

[7] A.I. Taponen, A. Ayadi, N. Svahn, M.K. Lahtinen, M. Rouzières, R. Clérac, H. M. Tuononen, A. Mailman, Role of Alkyl substituent and solvent on the structural, thermal, and magnetic properties of binary radical salts of 1,2,3,5-Dithia- or Diselenadiazolyl cations and the TCNQ anion, Cryst. Growth Des. 22 (2022) 7110–7122, https://doi.org/10.1021/acs.cgd.2c00.

[8] J. Zhang, W. Kosaka, Y. Kitagawa, H. Miyasaka, A host–guest electron transfer mechanism for magnetic and electronic modifications in a redox-active metal–organic framework, Angew. Chem. 134 (2022), e202115976, https://doi.org/10.1002/ange.202115976.

[9] P.W. Anderson, P.A. Lee, M. Saitoh, Remarks on giant conductivity in TTF-TCNQ, Solid State Commun. 13 (1973) 595–598, https://doi.org/10.1016/S0038-1098(73)80020-1.

[10] S. Matsuoka, K. Ogawa, R. Ono, K. Nikaido, S. Inoue, T. Higashino, M. Tanaka, J. Tsutsumi, R. Kondo, R. Kumai, S. Tsuzuki, S. Arai, T. Hasegawa, Highly stable and isomorphic donor–acceptor stacking in a family of n-type organic semiconductors of BTBT–TCNQ derivatives, J. Mater. Chem. C. 10 (2022) 16471–16479, https://doi.org/10.1039/d2tc03634g.

[11] A. Nafady, A.P. O'Mullane, A.M. Bond, Electrochemical and photochemical routes to semiconducting transition metal-tetracyanoquinodimethane coordination polymers, Coord. Chem. Rev. 268 (2014) 101–142.

[12] R. Basori, M. Kumar, A. Raychaudhuri, Sustained resistive switching in a single Cu: 7,7,8,8-tetracyanoquinodimethane nanowire: a promising material for resistive random access memory, Sci Rep 6 (2016) 26764, https://doi.org/10.1038/srep26764.

[13] H. Peng, S. Huang, D. Tranca, F. Richard, W. Baaziz, X. Zhuang, P. Samorì, A. Ciesielski, Quantum capacitance through molecular infiltration of 7,7,8,8-tetracyanoquinodimethane in metal−organic framework/covalent organic framework hybrids, ACS Nano 15 (2021) 18580–18589, https://doi.org/10.1021/acsnano.1c09146.

[14] R. Ramanathan, S. Walia, A.E. Kandjani, S. Balendran, M. Mohammadtaheri, S. K. Bhargava, K. Kalantar-zadeh, V. Bansal, Low-temperature fabrication of alkali metal−organic charge transfer complexes on cotton textile for optoelectronics and gas sensing, Langmuir 31 (2015) 1581–1587, https://doi.org/10.1021/la501446b.

[15] K. Wang, X. Qian, L. Zhang, Y. Li, H. Liu, Inorganic−organic p-n heterojunction nanotree arrays for a high-sensitivity diode humidity sensor, ACS Appl. Mater. Interfaces. 5 (2013) 5825–5831, https://doi.org/10.1021/am4014677.

[16] Z.M. Davoudi, A.E. Kandjani, A.I. Bhatt, I.L. Kyratzis, A.P. O'Mullane, V. Bansal, Hybrid antibacterial fabrics with extremely high aspect ratio Ag/AgTCNQ nanowires, Adv. Funct. Mater 24 (2014) 1047–1053, https://doi.org/10.1002/adfm.201302368.

[17] M. Mahajan, S.K. Bhargava, A.P. O'Mullane, Reusable surface confined semiconducting metal-TCNQ and metal-$TCNQF_4$ catalysts for electron transfer reactions, RSC Adv. 3 (2013) 4440–4446, https://doi.org/10.1039/c3ra22936j.

[18] A. Pearson, A.P. O'Mullane, S.K. Bhargava, V. Bansal, Synthesis of CuTCNQ/Au microrods by galvanic replacement of semiconducting phase I CuTCNQ with $KAuBr_4$ in aqueous medium, Inorg. Chem. 51 (2012) 8791–8801, https://doi.org/10.1021/ic300555j.

[19] X. Zhang, M.R. Saber, A.P. Prosvirin, J.H. Reibenspies, L. Sun, M. Ballesteros-Rivas, H. Zhaoa, K.R. Dunbar, Magnetic ordering in TCNQ-based metal–organic frameworks with host–guest interactions, Inorg. Chem. Front. 2 (2015) 904–911, https://doi.org/10.1039/c5qi00128e.

[20] D. Lee, L. Dong, Y.R. Kim, J. Kim, M. Lee, Y. Kim, Reduction-responsive supramolecular sheets for selective regulation of facultative anaerobe agglutination, Adv. Healthcare Mater. 12 (2023), 2203136, https://doi.org/10.1002/adhm.202203136.

[21] H. Zhao, R.A. Heintz, X. Ouyang, K.R. Dunbar, C.F. Campana, R.D. Rogers, Spectroscopic, thermal, and magnetic properties of Metal/TCNQ network polymers with extensive supramolecular interactions between layers, Chem. Mater. 11 (1999) 736–746, https://doi.org/10.1021/cm980608v.

[22] A. Berlie, I. Terry, S. Giblin, T. Lancaster, M. Szablewski, A muon spin relaxation study of the metal-organic magnet $Ni(TCNQ)_2$, J. App. Phys. 113 (2013) 17E304, https://doi.org/10.1063/1.4798616.

[23] A. Berlie, I. Terry, M. Szablewski, S.R. Giblin, Separating the ferromagnetic and glassy behavior within the metal-organic magnet $Ni(TCNQ)_2$, Phys. Rev. B. 92 (2015), 184431, https://doi.org/10.1103/PhysRevB.92.184431.

[24] A.J. Epstein, E.M. Conwell, D.J. Sandman, J.S. Miller, Electrical conductivity of-methyl phenazinium tetracyanoquinodimethanide, (NMP)(TCNQ), Solid State Commun. 23 (1977) 355–358, https://doi.org/10.1016/0038-1098(77)90231-9.

[25] C.R. Groom, I.J. Bruno, M.P. Lightfoot, S.C. Ward, The cambridge structural database, Acta Cryst B72 (2016) 171–179, https://doi.org/10.1107/S2052520616003954.

[26] L. Ballester, A. Gutiérrez, M.F. Perpiñán, U. Amador, M.T. Azcondo, A.E. Sánchez, C. Bellitto, Supramolecular architecture in Nickel(II) polyamine Tetracyanoquinodimethanido systems, Inorg. Chem. 36 (1997) 6390–6396, https://doi.org/10.1021/ic970851g.

[27] C. Alonso, L. Ballester, A. Gutiérrez, M.F. Perpiñán, A.E. Sánchez, M.T. Azcondo, Tetracyanoquinodimethanido derivatives of (Terpyridine)- and (Phenanthroline) metal complexes – structural and magnetic studies of radical-ion salts, Eur. J. Inorg. Chem. 3 (2005), https://doi.org/10.1002/ejic.200400540, 486-195.

[28] J. Černák, M. Hegedüs, L. Váhovská, J. Kuchár, D. Šoltésová, E. Čižmár, A. Feher, L. R. Falvello, Syntheses, crystal structures and magnetic properties of complexes based on $[Ni(L\text{-}L)_3]^{2+}$ complex cations with dimethylderivatives of 2,2-bipyridine

and TCNQ, Sol. State Scie. 77 (2018) 27–36, https://doi.org/10.1016/j.solidstatesciences.2018.01.004.
[29] D. Xue, Q.-Y. Lv, Ch.-N. Lin, S.-Z. Zhan, Function of 7,7,8,8-tetracyanoquinodimethane (TCNQ) on electrocatalytic hydrogen generation catalyzed by N,N′-benzene bis(salicylideniminato)nickel(II), Polyhedron 117 (2016) 300–308, https://doi.org/10.1016/j.poly.2016.05.064.
[30] T. Miyake, T. Ishida, D. Hashizume, F. Iwasaki, T. Nogami, Ferromagnetic S=1 chain formed by a square Ni_2S_2 motif in $Ni(qt)_2$ (qt = quinoline-8-thiolate). Magnetic properties of related compounds, Polyhedron 20 (2001) 1551–1555, https://doi.org/10.1016/S0277-5387(01)00653-2.
[31] J. Nishijo, A. Miyazaki, T. Enoki, Structure and physical properties of molecule-based magnets including transition metal complexes of crown thioethers, Bull. Chem. Soc. Jpn. 77 (2004) 715–727, https://doi.org/10.1246/bcsj.77.715.
[32] J.L. Shott, M.B. Freeman, N.-A. Saleh, D.S. Jones, D.W. Paley, Ch. Bejger, Ball and socket assembly of binary superatomic solids containing trinuclear nickel cluster cations and fulleride anions, Inorg. Chem. 56 (2017) 10984–10990, https://doi.org/10.1021/acs.inorgchem.7b01259.
[33] R.J. Butcher, E. Sinn, Synthesis and relation between magnetic and structural properties of series of monomeric and dimeric nickel(II) complexes. Crystal and molecular structure of $[Ni(biq)Cl_2]_2$, $Ni(biq)Br_2$, $[Ni(dmp)Cl_2]_2$, $[Ni(dmp)Br_2]_2$ and $Ni(bc)I_2$, Inorg. Chem. 16 (1977) 2334–2343, https://doi.org/10.1021/ic50175a037.
[34] C.-F. Ding, Y.-F. Miao, B.-Q. Tian, X.-M. Li, S.-S. Zhang, Aquadichloro(2,9-dimethyl-1,10-phenantroline-κ^2N,N′)nickel(II), Acta Cryst E62 (2006) m1062–m1063, https://doi.org/10.1107/S1600536806013250.
[35] A.M. Wright, G. Wu, T.W. Hayton, Formation of N_2O from Nickel Nitrosyl: isolation of cis-$[N_2O_2]^{2-}$ intermediate, J. Am. Chem. Soc. 134 (2012) 9930–9933, https://doi.org/10.1021/ja304204q.
[36] M. Uddin, M. Lalia-Kantouri, C.C. Hadjikostas, G. Voutsas, Synthesis and characterization of mixed-ligand Nickel(II) Chelates of β-Diones and α-Diimines. Crystal and molecular structure of $[Ni(ncup)_2Etacet]ClO_4$, Z. Anorg. Allg. Chem. 624 (1998) 1699–1705, 10.1002/(SICI)1521-3749(199810)624:10<1699::AID−ZAAC1699>3.0.CO;2-J.
[37] L.M. Toma, L.D. Toma, F.S. Delgado, C. Ruiz-Pérez, J. Sletten, J. Cano, J. M. Clemente-Juan, F. Lloret, M. Julve, Trans-dicyanobis(acetylacetonato)ruthenate (III) as a precursor to build novel cyanide-bridged Ru^{III}–M^{II} bimetallic compounds [M=Co and Ni], Coord. Chem. Rev. 250 (2006) 2176–2193, https://doi.org/10.1016/j.ccr.2005.11.018.
[38] E. Pardo, M. Verdaguer, P. Herson, H. Rousselière, J. Cano, M. Julve, F. Lloret, R. Lescouëzec, Synthesis, crystal structures and magnetic properties of a new family of heterometallic cyanide-bridged $Fe_2^{III}M_2^{II}$ (M=Mn, Ni and Co) square complexes, Inorg. Chem. 50 (2011) 6250–6262, https://doi.org/10.1021/ic200616p.
[39] S. Tanase, M. Ferbinteanu, M. Andruh, C. Mathoniére, I. Strenger, G. Rombaut, Synthesis and characterization of a new molecular magnet, $[Ni(ampy)_2]_3[Fe(CN)_6]_2{\cdot}6H_2O$, and synthesis, crystal structure and magnetic properties of its mononuclear precursor, trans-$[Ni(ampy)_2(NO_3)_2]$ (ampy =2-aminomethylpyridine), Polyhedron 19 (2000) 1967–1973, https://doi.org/10.1016/S0277-5387(00)00497-6.
[40] A.K. Chaudhari, B. Joarder, E. Riviére, G. Rogez, S.K. Ghosh, Nitrate-bridged "Pseudo-Double-Propeller"-Type Lanthanide(III)–Copper(II) heterometallic clusters: syntheses, structures, and magnetic properties, Inorg. Chem. 51 (2012) 9159–9161, https://doi.org/10.1021/ic3012876.
[41] S. Šterbinská, M. Holub, J. Kuchár, E. Čižmár, J. Černák, Markedly different magnetic properties of two analogous Ni(II) complexes with 2-aminoethylpyridine: $[Ni(2aepy)_2Cl(H_2O)]Cl{\cdot}H_2O$ and $[Ni(2aepy)_2(NO_3)]NO_3$, Polyhedron 187 (2020), 114654, https://doi.org/10.1016/j.poly.2020.114654.
[42] C.-F. Ding, M.-L. Zhang, X.-M. Li, S.-S. Zhang, Aqua(2,9-dimethyl-1,10-phenanthroline-κ^2N,N′)-dinitratocobalt(II), Acta Cryst. E62 (2006) m2540–m2542, https://doi.org/10.1107/S1600536806036476.
[43] S. Talebi, A. Abedi, V. Amani, Cobalt(II) complexes with small variations in the heterocycle ligand, crystal structure and DFT calculations, J. Mol. Struc. 1230 (2021), 129911, https://doi.org/10.1016/j.molstruc.2021.129911.
[44] S. Šterbinská, M. Holub, E. Čižmár, J. Černák, L.R. Falvello, M. Tomás, An old crystallization technique as a fast, facile and adaptable method for obtaining single crystals of unstable "Li_2TCNQF_4" and new compounds of TCNQ or $TCNQF_4$: syntheses, crystal structures and magnetic properties, Cryst. Growth Des. 23 (2023) 4357–4369, https://doi.org/10.1021/acs.cgd.3c00160.
[45] Oxford Diffraction, CrysAlis RED and CrysAlis CCD Software (Ver. 1.171.38.41), Rigaku Oxford Diffraction Ltd, Abingdon, Oxfordshire, England, 2015.
[46] R.H. Blessing, An empirical correction for absorption anisotropy, Acta Cryst. A51 (1995) 33–38, https://doi.org/10.1107/S0108767394005726.
[47] G.M. Sheldrick, SHELXT - Integrated space-group and crystal-structure determination, Acta Cryst A71 (2015) 3–8, https://doi.org/10.1107/S2053273314026370.
[48] G.M. Sheldrick, Crystal structure refinement with SHELXL, Acta Cryst. C71 (2015) 3–8, https://doi.org/10.1107/S2053229614024218.
[49] L.J. Farrugia, WinGX and ORTEP for Windows: an update, J. Appl. Cryst. 45 (2012) 849–854, https://doi.org/10.1107/S0021889812029111.
[50] K. Brandenburg, Crystal Impact (Version 3.1f) GbR, DIAMOND, 2008. Bonn, Germany.
[51] ChemSketch, Version 2022.1.2, Advanced Chemistry Development, Inc. (ACD/Labs), Toronto, ON, Canada, www.acdlabs.com.
[52] C.F. Macrae, I. Sovago, S.J. Cottrell, P.T.A. Galek, P. McCabe, E. Pidcock, M. Platings, G.P. Shields, J.S. Stevens, M. Towler, P.A. Wood, Mercury 4.0: from visualization to analysis, design and prediction, J. Appl. Cryst. 53 (2020) 226–235, https://doi.org/10.1107/S1600576719014092.
[53] K. Nakamoto, Infrared and Raman Spectra of Inorganic and Coordination Compounds, 6th ed., Wiley, New York, 2009.
[54] P. Sharma, P. Sarma, A. Frontera, M. Barceló-Oliver, A.K. Verma, B. Sarma, R. Barthakur, M.K. Bhattacharyya, Energetically significant cooperative π-stacked ternary assemblies in Ni(II) phenanthroline compounds involving discrete water clusters: anticancer activities and theoretical studies, J. Mol. Struc. 1229 (2021), 129486, https://doi.org/10.1016/j.molstruc.2020.129486.
[55] L. Krešáková, A. Miňo, M. Holub, J. Kuchár, A. Werner, M. Tomás, E. Čižmár, L. R. Falvello, J. Černák, Heteroleptic complexes of Ni(II) with 2,2′-bipyridine and benzoate ligands. Magnetic properties of $[Ni(bpy)(Bz)_2]$, Inorganica Chim. Acta. 527 (2021), 120588, https://doi.org/10.1016/j.ica.2021.120588.
[56] C.-F. Ding, Y.-Q. Yu, M.-L. Zhang, X.-M. Li, S.-S. Zhang, Aqua(2,9-dimethyl-1,10-phenanthroline-κ^2N,N′)-dinitratoiron(II), Acta. Cryst. E62 (2006) m1871–m1872, https://doi.org/10.1107/S1600536806027139.
[57] N. El-Azzouzi, F. Huesco-Ureña, N.A. Illán-Cabeza, M.N. Moreno-Carretero, XRD structure of two heptacoordinated Mn(II) complexes containing 2,9-dimethyl-1,10-phenanthroline (phen), nitrato and nicotinato bidentate anions: $[Mn(phen)(nicot)(NO_3)(H_2O)]{\cdot}EtOH{\cdot}H_2O$ and $[Mn(phen)(NO_3)_2(H_2O)]$, Polyhedron 29 (2010) 1405–1410, https://doi.org/10.1016/j.poly.2010.01.026.
[58] B. Cordero, V. Gómez, A.E. Platero-Prats, M. Revés, J. Echeverría, E. Cremades, F. Barragán, S. Alvarez, Covalent radii revisited, Dalton Trans 21 (2008) 2832–2838, https://doi.org/10.1039/B801115J.
[59] M.C. Etter, J.C. MacDonald, Graph-set analysis of hydrogen-bond patterns in organic crystals, Acta Cryst B46 (1990) 256–262, https://doi.org/10.1107/S0108768189012929.
[60] A. Uhrinová, J. Kuchár, A. Orendáčová, M. Pitoňák, J. Federič, J. Noga, J. Černák, $[Ni(bpy)(mal)(H_2O)_3]{\cdot}H_2O$ and $[Ni(4,4'\text{-dmbpy})(mal)(H_2O)_3]{\cdot}1{\cdot}5H_2O$: syntheses, crystal structures, magnetic properties, and computational study of stacking interactions, J. Coord. Chem. 70 (2017) 2999–3018, https://doi.org/10.1080/00958972.2017.1376738.
[61] T.J. Kistenmacher, T.J. Emge, A.N. Bloch, D.O. Cowan, Structure of the red, semiconducting form of 4,4′,5,5′-tetramethyl-$\Delta^{2,2'}$-bi-1,3-diselenole-7,7,8,8-tetracyano-*p*-quinodimethane, TMTSF-TCNQ, Acta Cryst. B38 (1982) 1193–1199, https://doi.org/10.1107/S0567740882005275.
[62] J.P. Peterson, A.H. Winter, Solvent-responsive radical dimers, Org. Lett. 22 (2020) 6072–6076, https://doi.org/10.1021/acs.orglett.0c02152.
[63] S.K. Hoffmann, P.J. Corvan, P. Singh, C.N. Sethulekshmi, R.M. Metzger, W. E. Hatfield, Crystal structure and excited triplet-state electron paramagnetic resonance of the σ-Bonded TCNQ Dimer in Bis(2,9-dimethyl-1,10-phenanthroline) copper(I) Tetracyanoquinodimethanide, $[Cu(DMP)_2]_2[TCNQ]_2$, J. Am. Chem. Soc. 105 (1983) 4608–4617, https://doi.org/10.1021/ja00352a016.